Ⅳ 研究成果の刊行物・別刷

THE JOURNAL OF BIOLOGICAL CHEMISTRY VOL. 282, NO. 14, pp. 10731–10741, April 6, 2007

Roles of Hemoglobin Allostery in Hypoxia-induced Metabolic Alterations in Erythrocytes

SIMULATION AND ITS VERIFICATION BY METABOLOME ANALYSIS[*] [S]

Received for publication, November 20, 2006, and in revised form, January 29, 2007 Published, JBC Papers in Press, February 8, 2007, DOI 10.1074/jbc.M610717200

Ayako Kinoshita[‡1], Kosuke Tsukada[§], Tomoyoshi Soga[‡], Takako Hishiki[§2], Yuki Ueno[‡], Yoichi Nakayama[‡], Masaru Tomita[‡], and Makoto Suematsu[§3]

From the [‡]Institute for Advanced Biosciences, Keio University, Tsuruoka, Yamagata 997-0017, Japan and [§]Department of Biochemistry and Integrative Medical Biology, School of Medicine, Keio University, Shinanomachi, Shinjuku-ku, Tokyo 160-8582, Japan

When erythrocytes are exposed to hypoxia, hemoglobin (Hb) stabilizes in the T-state by capturing 2,3-bisphosphoglycerate. This process could reduce the intracellular pool of glycolytic substrates, jeopardizing cellular energetics. Recent observations suggest that hypoxia-induced activation of glycolytic enzymes is correlated with their release from Band III (BIII) on the cell membrane. Based on these data, we developed a mathematical model of erythrocyte metabolism and compared hypoxia-induced differences in predicted activities of the enzymes, their products, and cellular energetics between models with and without the interaction of Hb with BIII. The models predicted that the allostery-dependent Hb interaction with BIII accelerates consumption of upstream glycolytic substrates such as glucose 6-phosphate and increases downstream products such as phosphoenolpyruvate. This prediction was consistent with metabolomic data from capillary electrophoresis mass spectrometry. The hypoxia-induced alterations in the metabolites resulted from acceleration of glycolysis, as judged by increased conversion of [^{13}C]glucose to [^{13}C]lactate. The allostery-dependent interaction of Hb with BIII appeared to contribute not only to maintenance of energy charge but also to further synthesis of 2,3-bisphosphoglycerate, which could help sustain stabilization of T-state Hb during hypoxia. Furthermore, such an activation of glycolysis was not observed when Hb was stabilized in R-state by treating the cells with CO. These results suggest that Hb allostery in erythrocytes serves as an O_2-sensing trigger that drives glycolytic acceleration to stabilize intracellular energetics and promote the ability to release O_2 from the cells.

Erythrocytes deliver molecular oxygen (O_2) to tissues through allosteric regulation of hemoglobin (Hb). The ability of Hb to release O_2 is determined by a variety of metabolites in the intracellular compartment, such as protons (H^+), 2,3-bisphosphoglycerate (2,3-BPG),[4] nitric oxide (NO), and ATP. The decrease in H^+ and the increase in the aforementioned compounds (2,3-BPG, NO, and ATP) stabilize the T-state of Hb, thereby facilitating O_2 dissociation from the cells. In contrast, O_2 and carbon monoxide (CO) function as positive allosteric effectors that stabilize Hb in its R-state and down-regulate O_2 dissociation. When exposed to hypoxic conditions, erythrocytes are known to accelerate glucose consumption (1). This event appears to result from acceleration of glycolysis, as judged by the increase in 2,3-BPG (2), a metabolite stabilizing the T-state of Hb. Because T-state Hb has a higher affinity to 2,3-BPG and ATP than the R-state Hb, stabilization of the former structure would reduce amounts of free ATP available for maintenance of cellular homeostasis. ATP is consumed continuously by various ATPases to maintain ionic homeostasis and by adenylate cyclase to generate cyclic AMP to maintain the deformability of the cells. Upon hypoxia, a fraction of the intracellular ATP is released to the extracellular space to elicit hypoxia-induced vasorelaxation, although the actual amounts of ATP released seem small compared with levels within the cell (3). Furthermore, the cells require ATP in the initial steps of glycolysis (*e.g.* used by hexokinase (HK) and phosphofructokinase (PFK)) to trigger ATP synthesis. These features have led researchers to hypothesize that erythrocytes might have mechanisms for responding quickly to hypoxia to up-regulate *de novo* ATP synthesis.

There is a growing body of evidence showing that the interaction of Hb with Band III (BIII), a major transmembrane protein in erythrocytes, plays a role in these compensatory mechanisms to maintain intracellular ATP levels (4–6). BIII, also known as anion exchanger type I, accounts for about 25% of the total erythrocyte membrane protein (7), and its cytoplasmic domain displays a greater affinity for Hb

* This work was supported by JSPS Grant-in-aid for Creative Scientific Research Grant 17GS0419 and in part by a grant from New Energy and Industrial Technology Development Organization. Development of the basic software (E-Cell) was supported by grants from Japan Science and Technology Corp. and from Yamagata Prefecture. Development of computer-based biosimulation for erythrocyte metabolism was supported by Leading Project for Biosimulation from MEXT. The costs of publication of this article were defrayed in part by the payment of page charges. This article must therefore be hereby marked "*advertisement*" in accordance with 18 U.S.C. Section 1734 solely to indicate this fact.

[S] The on-line version of this article (available at http://www.jbc.org) contains supplemental material.

[1] Research associate supported by 21st Century Center-of-Excellence Program from the Ministry of Education, Culture, Sports, Science, and Technology.

[2] Research fellow supported by Grant-in-aid for Creative Scientific Research Grant 17GS0419.

[3] To whom correspondence should be addressed. E-mail: msuem@sc.itc.keio.ac.jp.

[4] The abbreviations used are: 2,3-BPG, 2,3-bisphosphoglycerate; CE-MS, capillary electrophoresis mass spectrometry; PK, pyruvate kinase; HK, hexokinase; PFK, phosphofructokinase; ALD, aldolase; GAPDH, glyceraldehyde-3-phosphate dehydrogenase; LDH, lactate dehydrogenase; G6P, glucose 6-phosphate; F6K, fructose 6-phosphate; DHAP, dihydroxyacetone phosphate; 3PG, 3-phosphoglycerate; PEP, phosphoenolpyruvate; F1,6BP, fructose 1,6-bisphosphate; BIII, Band III.

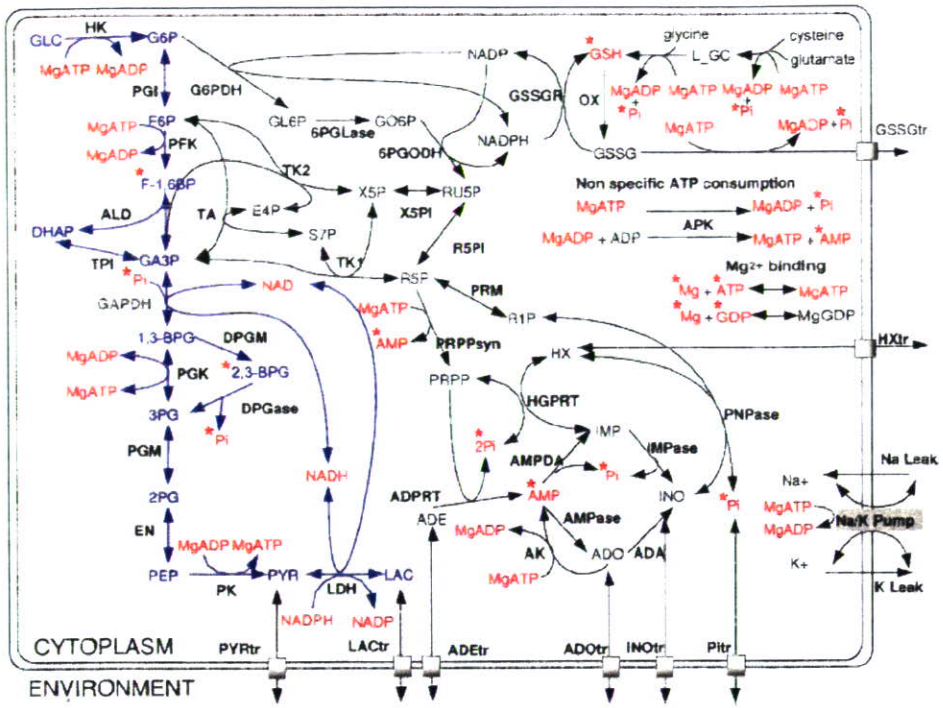

FIGURE 1. **Metabolic pathways included in the mathematical model.** *Blue*, glucose-derived carbon flux in glycolysis. *Red*, substrates or allosteric effectors of glycolytic enzymes, including adenine nucleotides, inorganic phosphates, and glutathione. Metabolites with *asterisks* indicate allosteric effectors of glycolytic enzymes. The mathematical model developed in this paper is composed of 46 enzymatic reactions, 11 membrane transport or ion pump systems, 37 reversible binding processes, and 1 allosteric hemoglobin transition. The model includes 61 metabolic intermediates whose steady-state levels are shown schematically in Table 1 and 36 protein-metabolite or protein-protein complexes as variables. In this figure the reactions indicating the catalytic processes of HK, PFK, and PK are described as apparently irreversible ones by a *one-headed arrow* for the principles of thermodynamics (44), whereas the kinetic equations used in the model are reversible in reality (see the supplemental data).

in the T-state rather than the R-state (8). BIII also binds to PFK (9), aldolase (ALD) (10), glyceraldehyde-3-phosphate dehydrogenase (GAPDH) (11), and lactate dehydrogenase (LDH) (12). Recent observations have shown that these enzymes reduce their catalytic activities upon binding to BIII, and activity is recovered upon dissociation from BIII as free forms (13, 14). These results led us to hypothesize that Hb stabilized in the T-state upon hypoxia serves as a trigger to increase the activity of glycolytic enzymes and to accelerate glucose consumption to increase ATP synthesis. Several reports to date have provided circumstantial evidence showing hypoxia-induced activation of glycolysis by measuring glycolytic intermediates in erythrocytes (15, 16). However, the mechanistic features of the coordination and dynamics of sequential glycolytic reactions and the outcomes in terms of alterations in intracellular metabolites are not comprehensively understood.

The aim of this study was to develop a dynamic mathematical model of metabolism in erythrocytes involving the O_2-sensing mechanisms of Hb, to predict temporal alterations in intracellular metabolites and cellular energetics in response to hypoxia, and to verify the predictions derived from the model through metabolome analyses. The differential equations of metabolic reactions used in the model are partially based on previous mathematical models for glycolytic metabolism in human erythrocytes (17, 18), for the pentose phosphate pathway, and for adenine nucleotide metabolism (19–22). In contrast to previous models, we first attempted to include the effects of BIII interactions with Hb and the glycolytic enzymes. The effects of inorganic phosphates and adenine nucleotides that could serve as allosteric effectors of glycolysis were included in the model, similar to recent mathematical models of erythrocytes (23, 24). The temporal alterations in metabolites predicted in the updated dynamic mathematical model are in good agreement with results obtained from the metabolome analyses using capillary electrophoresis mass spectrometry, which has recently emerged as a powerful tool for the global analysis of charged metabolites (25, 26). In contrast, the virtual model lacking the effects of the Hb-BIII interaction was unable to reproduce actual alterations in the metabolites, suggesting a pivotal role for this molecular interaction in the maintenance of erythrocyte energetics.

MATERIALS AND METHODS

Mathematical Model of Human Erythrocyte Metabolism—All numerical calculations were performed using the E-Cell 3 simulation environment (27, 28). The model can be found in the supplemental data. It provides rate equations and the relevant parameters for all processes included in the model.

Description of the Metabolic Model—We developed a mathematical model of human erythrocyte metabolism (Fig. 1) with kinetic descriptions of reaction rates derived from previously published experimental data and partially from those based on published models, as depicted in detail in the supplemental data. The metabolic reactions included in the developed model are listed in Table 1, and the abbreviations of enzymes and compounds are shown in Tables 1 and 2, respectively. Our mathematical model not only included the glycolytic pathway but also comprised other metabolic pathways that are directly or indirectly related to regulatory mechanisms for glycolysis. The pentose monophosphate shunt, adenine nucleotide metabolism, and the salvage pathway including hypoxanthine-guanine phosphoribosyltransferase were included, since these components determine levels of AMP and P_i, which are known regulators of PFK and GAPDH, respectively (*asterisks* in Fig. 1). Another important component we included is the *de novo* synthesis and transport of glutathione. This compound occurs at millimolar levels in the cell, and its synthesis and transport are significant energy-consuming processes. Furthermore, GSH serves as a regulator of HK. The Na^+/K^+ pump consumes large

TABLE 1
Enzymatic reactions included in the model

Enzyme/Process	Abbreviation	Substrates		Products	Effectors
Hexokinase	HK	GLC + MgATP	→	G6P + MgADP	2, 3-BPG, GDP, GSH
Phosphoglucoisomerase	PGI	G6P	⟷	F6P	
Phosphofructokinase	PFK	F6P + MgATP	→	F-1,6BP + MgADP	fATP, Mg, 2, 3-BPG fAMP, Phos, GDP
Aldolase	ALD	F-1,6BP	⟷	DHAP + GA3P	2, 3-BPG, Mg2, 3-BPG
Triose phosphate isomerase	TPI	DHAP	⟷	GA3P	
Glyceraldehyde phosphate dehydrogenase	GAPDH	GA3P + Phos + NAD	⟷	1,3-BPG + NADH	
Diphosphoglycerate mutase	DPGM	1,3-BPG	→	2,3-BPG	
Diphosphoglycerate phosphatase	DPGase	2,3-BPG	→	P3GA + Phos	
Phosphoglycerate kinase	PGK	1,3-BPG + MgADP	⟷	P3GA + MgATP	
Phosphoglyceromutase	PGM	P3GA	⟷	P2GA	
Enolase	EN	P2GA	⟷	PEP	Mg
Pyruvate kinase	PK	PEP + MgADP	⟷	PYR + MgATP	fATP, F-1, 6BP, GDP
Lactate dehydrogenase	LDH	PYR + NADH	→	LAC + NAD	
Lactate dehydrogenase (NADPH)	LDHP	PYR + NADPH	→	LAC + NADP	
Glucose 6-phosphate dehydrogenase	G6PDH	NADP + G6P	→	GL6P + NADPH	MgATP, 2, 3-BPG
6-Phosphogluconolactonase	6PGLase	GL6P	→	GO6P	
6-Phosphogluconate dehydrogenase	6PGODH	GO6P + NADP	⟷	RU5P + NADPH + CO_2	
Transaldolase	TA	S7P + GA3P	→	E4P + F6P	
Transketolase I	TK1	X5P + R5P	→	GA3P + S7P	
Transketolase II	TK2	X5P + E4P	→	GA3P + F6P	
Ribose-5-phosphate isomerase	R5PI	RU5P	→	R5P	
Xylulose-5-phosphate isomerase	X5PI	RU5P	→	X5P	
γ-Glutamyl systeine synthetase	L_GCS	MgATP + glutamate + cysteine	⟷	MgADP + L_GC + Phos	GSH
Glutathione synthetase	GSH_S	L_GC + glycine + MgATP	⟷	GSH + MgADP + Phos	
Glutathione reductase (NADPH)	GSSGR	GSSG + NADPH	→	GSH + NADP	
Adenosine deaminase	ADA	ADO	⟷	INO	
Adenine phosphoribosyl transferase	ADPRT	ADE + PRPP	→	fAMP + 2Phos	
Adenosine kinase	AK	ADO + MgATP	⟷	MgADP + fAMP	
Adenosine monophosphate deaminase	AMPDA	fAMP	→	IMP	
AMP phosphohydrolase	AMPase	fAMP	⟷	ADO + Phos	
Adenylate kinase	APK	fADP + MgADP	→	fAMP + MgATP	
Hypoxanthine-guanine phosphoryl transferase	HGPRT	PRPP + HXi	→	IMP + 2Phos	
Inosine monophosphatase	IMPase	IMP	⟷	INO + Phos	
Purine nucleotide phosphorylase	PNPase	INO + Phos	→	HXi + R1P	
Phosphoribosyl pyrophosphate synthetase	PRM	R1P	→	R5P	
Phosphoribosyl pyrophosphate synthetase	PRPPsyn	R5P + MgATP	→	PRPP + fAMP + Mg	
Adenosine triphosphate phosphohydrolase	ATPase	MgATP	→	MgADP + Phos	
Glutathione turnover	OX	2GSH	→	GSSG	
Non-glycolytic NADH consumption process	OXNADH	NADH	→	NAD	
Adenine transport process	ADEtr	ADE	→	ADEe	
Adenosine transport process	ADOtr	ADO	→	ADOe	
Hypoxanthine transport process	HXtr	HXi	→	HXe	ADEe
Inosine transport process	INOtr	INO	→	INOe	
Leak of potassium	K_Leak	Ke	⟷	Ki	
Lactate transport process	LACtr	LAC	→	LACe	
Sodium/potassium pump	NaK_Pump	3Nai + 2Ke + MgATP	→	3Nae + 2Ki + MgADP + Phos	
Leak of sodium	Na_Leak	Nae	→	Nai	
Pyruvate transport process	PYRtr	PYR	→	PYRc	
Inorganic phosphate transport process	Phostr	Phos	→	Phose	
GSSG transport process	GSSG transport	GSSG + MgATP	⟷	GSSGe + MgADP + Phos	

amounts of MgATP and is modeled using precise kinetic equations described elsewhere. We also considered the effects of magnesium ion (Mg^{2+}) binding to ATP, ADP, AMP, 1,3-BPG, 2,3-BPG, F1,6BP, and GDP using the respective binding affinities shown in the supplemental Table 1. Because it is now assumed that enzymes employ the complexed form of ATP (MgATP or MgADP) as substrates, these binding processes are important to be considered. Transport of metabolites such as Ade, Ado, Ino, hypoxanthine, and lactate were modeled under the assumption that they move across the membrane simply according to their concentration gradient between intra- and extracellular spaces. Thus, the diagram shown in Fig. 1 constitutes a mathematical model including 83 different chemical reactions and 11 transporter functions that cover a majority of the metabolic pathways influencing the concentrations of allosteric effectors and/or substrates for glycolysis.

Modeling BIII-mediated Interactions between Hb and Glycolytic Enzymes—Reversible binding of the glycolytic enzymes (PFK, ALD, GAPDH) and two allosteric forms of Hb (R- and T-states) to BIII on the membrane were modeled in the current study on the basis of the individual association constants listed in Table 3. T-state Hb has a 100-fold greater affinity to BIII and is much more likely to associate with this anion transporter than R-state Hb. The catalytic activities of PFK, ALD, and GAPDH are inhibited through their specific binding to BIII, but formation of such complexes appeared to be reversible (13). Based on these findings in the model, these enzymes were assumed to be completely inactivated upon formation of the complex and activated reversibly upon dissociation. Under these circumstances the competitive association of Hb and the glycolytic enzymes with BIII and the resultant changes in glycolysis could occur in response to alterations in partial O_2 tension (pO_2 mm Hg).

TABLE 2

Steady-state concentrations of metabolic intermediates in human erythrocytes in normoxia: concentrations were predicted by the model and observed *in vivo*

Metabolite	Abbreviation	Concentration	
		Model	Literature
		mM	
Glucose 6-phosphate	G6P	6.0E−02	3.8E−02[a], 3.9E−02[b]
Fructose 6-phosphate	F6P	1.9E−02	1.6E−02[a]
Fructose 1,6-bisphosphate	F-1,6BP	5.6E−03	7.6E−03[a], 2.7E−03[b]
Dihydroxyacetone phosphate	DHAP	1.5E−02	1.4E−02[a]
Glyceraldehyde 3-phosphate	GA3P	3.6E−03	4.0E−03[c], 5.7E−03[b]
1,3-Bisphosphoglycerate	1,3-BPG	2.3E−04	4.0E−04[a]
3-Phosphoglycerate	3PG	4.8E−02	4.5E−02[a], 5.4E−02[c]
2-Phosphoglycerate	2PG	1.4E−02	1.4E−02[a]
Phosphoenolpyruvate	PEP	8.1E−03	1.7E−02[a]
Pyruvate	PYR	5.2E−02	5.0E−02[c], 7.7E−02[a]
Lactate	LAC	1.3E+00	1.1E−03[a], 1.4E−03[b]
Gluconolactone 6-phosphate	GL6P	5.3E−06	
Gluconate 6-phosphate	GO6P	4.5E−02	
Ribulose 5-phosphate	RU5P	4.9E−03	
Sedoheptulose 7-phosphate	S7P	2.1E−02	
Xylulose 5-phosphate	X5P	9.0E−03	
Erythrose 4-phosphate	E4P	4.5E−04	
Ribose 5-phosphate	R5P	5.8E−03	
Ribose 1-phosphate	R1P	8.1E−02	6.0E−02[a]
5-Phosphoribosyl 1-phosphate	PRPP	1.4E−03	5.0E−03[a]
Inosine monophosphate	IMP	8.1E−03	5.7E−03[d]
Inosine	INO	1.5E−04	1.0E−03[a]
Adenine	ADE	1.5E−02	1.3E−02[e]
Adenosine	ADO	4.5E−05	
Hypoxanthine	HX	1.6E−03	2.0E−03[a]
L-glutamyl cysteine	L_GC	4.2E−04	
Glutathione (reduced)	GSH	3.3E+00	3.2E+00[a,b]
Glutathione (oxidized)	GSSG	4.7E−03	6.0E−03[b]
Nicotinamide adenine dinucleotide	NAD	6.5E−02	6.2E−02[a]
Nicotinamide adenine dinucleotide	NADH	2.8E−04	
Nicotinamide adenine phosphate	NADP	6.5E−05	
Nicotinamide adenine phosphate	NADPH	6.5E−02	6.6E−02[a]
Potassium ion	Ki	1.3E+02	1.4E+02[b]
Sodium ion	Nai	3.4E+01	1.0E+01[a]
Inorganic phosphate	Phos	1.0E+00	1.0E+00[b]
Total adenosine diphosphate	tADP	3.3E−01	3.1E−01[b]
Total adenosine monophosphate	tAMP	3.4E−02	3.0E−02[b]
Total adenosine triphosphate	tATP	1.9E+00	2.1E+00[b]
Total 2,3-bisphosphoglycerate	t2,3-BPG	3.7E+00	4.5E+00[a]

[a] Reported by Joshi and Palsson (22).
[b] Reported by Mulquiney and Kuchel (24).
[c] From Ref. 45.
[d] From Ref. 46.
[e] From Ref. 47.

TABLE 3

Association constants of Hbs and glycolytic enzymes to BIII

Proteins	*Ka*
	/M
Deoxyl-Hb	10000[a]
Oxy-Hb	100[a]
PFK	5,000,000[b]
ALD	1,000,000[c]
GAPDH	2,000,000[c]

[a] From Ref. 48.
[b] From Ref. 49.
[c] From Ref. 40.

Thus, in this mathematical model we were able to manipulate pO_2, an independent variable of the model, as a parameter and to predict glycolytic metabolism as a dependent variable. Another important assumption is that pO_2 alters the T-R transition of Hb according to a reversible Hill-type equation (29) that is also dictated by pCO_2 levels, intracellular pH, concentrations of 2,3-BPG and ATP, and temperature (supplemental data, page 8–9).

Perturbations Mimicking Hypoxia—The aforementioned mathematical model was able to stably achieve individual steady states under varied pO_2 conditions over the range of 0–100 mm Hg. Because we aimed to predict metabolic alterations in response to hypoxia with this model, pO_2 was initially set to 100 mm Hg, a physiological value in alveoli (30). Under these conditions the basal and initial steady-state concentrations were calculated by this model, as depicted in Table 2 and supplemental Table 2. The external parameters, including environmental concentrations of metabolites and initial settings in the model, are listed in supplemental Table 3. To adapt the model to hypoxic conditions, pO_2 was reduced to 30 mm Hg, a value measured in capillary microvessels *in vivo* (30, 31), for the desired lengths of time. As seen in previous studies (30, 31), circulating erythrocytes may be exposed to such a pO_2 value when they travel through capillaries under physiological conditions (30) or when they traverse low-flow or static microvessels belonging to post-ischemic damaged regions in the liver (31). This protocol allowed us to remodel glycolytic metabolism in erythrocytes for the aforementioned circumstances.

Preparation of Human Erythrocytes for CE-MS Analysis—Erythrocytes were isolated from heparinized venous blood sam-

ples collected from healthy male volunteers according to our previous methods (31). Briefly, the samples were centrifuged at 2000 × *g* at 4 °C for 10 min, and the cells were washed 3 times and suspended in Tris buffer, pH 7.4, to adjust hematocrit values to 15%. The cell suspension was divided into hypoxic and normoxic groups. For the hypoxic group the cells were incubated in a gas-tight glass bottle and followed by a gentle purge with highly purified argon gas for 45 min at 4 °C. Cell samples (2 ml) were transferred to glass tubes on ice in an O_2-excluding chamber and finally incubated at 37 °C for 0, 0.5, 1, and 3 min. The reactions were terminated by cooling the sample-containing glass tubes with ice-cold water at 4 °C. The cells for normoxic controls were incubated similarly to the hypoxic group but treated by purging for 45 min with air instead of argon gas and finally incubated at 37 °C for 0, 0.5, 1, and 3 min. Likewise, the reactions were terminated at 4 °C by cooling in ice-cold water. For measurements at 0 min, the cells were incubated at 37 °C and immediately treated on ice to terminate the reaction. The present protocol for treating erythrocytes with argon gas allowed us to set up reproducible hypoxic conditions where the pO_2 was ~30 mm Hg.

The cell samples for these two groups were purified by centrifuging at 2000 × *g* at 4 °C for 10 min, and the pellets were treated with 0.16 ml of cold methanol containing 300 μM L-methionine sulfate for deproteination. L-Methionine sulfate was used as the internal standard to validate the recovery or loss of metabolites during sample preparation and CE-MS analysis (25). Next, 0.16 ml of chloroform and 0.08 ml of distilled water was added and thoroughly mixed. The solution was centrifuged at 12,000 × *g* at 4 °C for 15 min, and the upper aqueous layer was filtered through a centrifugal filter (Millipore 5-kDa NMWL) to remove proteins. The filtrate was analyzed by CE-MS. Metabolome data collected from erythrocytes exposed to hypoxia for the aforementioned times were plotted as relative concentrations *versus* the 3-min normoxic controls (see below). In some experiments erythrocytes were pretreated by an incubation with buffer saturated with CO, a stabilizer of R-state Hb. This incubation was performed for 20 min before the 45-min normoxic incubation time at 4 °C.

In a separate sets of experiments we examined the effects of the aforementioned procedure of hypoxia on the conversion of [$^{13}C_6$]glucose to [$^{13}C_3$]lactate in human erythrocytes. In these experiments erythrocytes isolated from venous blood samples were suspended in buffer to adjust hematocrit values to 30%. The cell suspension was divided into hypoxic and normoxic samples to be treated by purging for 45 min at 4 °C with argon and air, respectively. Cell samples (1 ml) were then transferred to glass tubes containing 1 ml of buffer containing 5 mM [$^{13}C_6$]glucose, giving a final hematocrit value of 15%. Immediately after mixing at 4 °C, the samples were incubated at 37 °C for 3 min, and the reactions were terminated at 4 °C by immersion in ice-cold water. Preparation of cell pellets and samples to determine the amount of $^{13}C_3$-labeled lactate was identical to that for conventional metabolome analyses, as described below and elsewhere (26). The flux indicating the conversion of [$^{13}C_6$]glucose to [$^{13}C_3$]lactate was determined as values relative to the amount of L-methionine sulfate in the samples added as an internal control. Using the same samples, [$^{13}C_3$]2,3-BPG was also determined when necessary.

Sample Recovery of Metabolome Analysis by CE-MS—Hb has the ability to capture intracellular metabolites such as 2,3-BPG and ATP. Additionally, deproteinization with cold methanol before processing for CE-MS analysis could cause loss of some of these metabolites through binding to denatured Hb. To quantify the putative loss of such metabolites, 2,3-BPG, ATP, glucose 6-phosphate (G6P), lactate, or α-ketoglutarate were incubated for 3 min at a final concentration of 300 μM (2,3-BPG) or 100 μM (other metabolites) in buffer containing 300 μM purified human Hb. To examine differences in the loss of these metabolites between T- and R-state Hb, the sample mixture was purged for 60 min with purified argon gas or with air, respectively, in the presence of 1 mg/ml sodium dithionite. Purified Hb solution was generously provided by Oxygenix Co. Ltd., Tokyo, Japan. The samples for CE-MS analysis were prepared as described above.

Instrumentation—All CE-MS experiments were performed using an Agilent CE Capillary Electrophoresis System equipped with an air pressure pump, an Agilent 1100 series MSD mass spectrometer and an Agilent 1100 series isocratic high performance liquid chromatography pump, a G1603A Agilent CE-MS adapter kit, and a G1607A Agilent CE-MS sprayer kit (Agilent Technologies). System control, data acquisition, and MSD data evaluation were performed using G2201AA Agilent ChemStation software for CE-MSD.

CE-MS Conditions for Anionic Metabolites—A cationic polymer coated SMILE (+) capillary was obtained from Nacalai Tesque (Kyoto, Japan) and used as the separation capillary (50-μm inner diameter × 100-cm total length). The electrolyte for the CE separation was 50 mM ammonium acetate solution, pH 8.5. Samples were injected with a pressure injection of 50 mbar for 30 s (30 nl). The applied voltage was set at −30 kV. ESI-MS was conducted in the negative ion mode, and the capillary voltage was set at 3500 V. For MS using the selective ion monitoring mode, deprotonated [M-H] ions were monitored for anionic metabolites of interest (32).

CE-MS Conditions for Nucleotides and Coenzyme A Compounds—Separations were carried out on a gas chromatograph capillary, polydimethylsiloxane (DB-1) (50-μm inner diameter × 100-cm total length) (Agilent Technologies). The electrolyte for the CE separation was 50 mM ammonium acetate, pH 7.5. The applied voltage was set at −30 kV, and a pressure of 50 mbar was added to the inlet capillary during the run to maintain a conductive liquid junction at the capillary outlet. All other conditions were the same as in the anionic metabolite analysis (32).

Calculation of Energy Charge in the Mathematical Model—Based on the definition proposed by Atkinson and Walton, an energy charge was calculated as an index of contents of high energy phosphate bonds in adenylate in the BIII(+) and BIII(−) models (33, 34). Energy charge is defined as one-half the number of anhydride-bound phosphates per adenylate moiety: energy charge = (ATP + ½ADP)/(AMP + ADP + ATP). With this parameter, the energy potential of an erythrocyte may vary from 0 to 1.

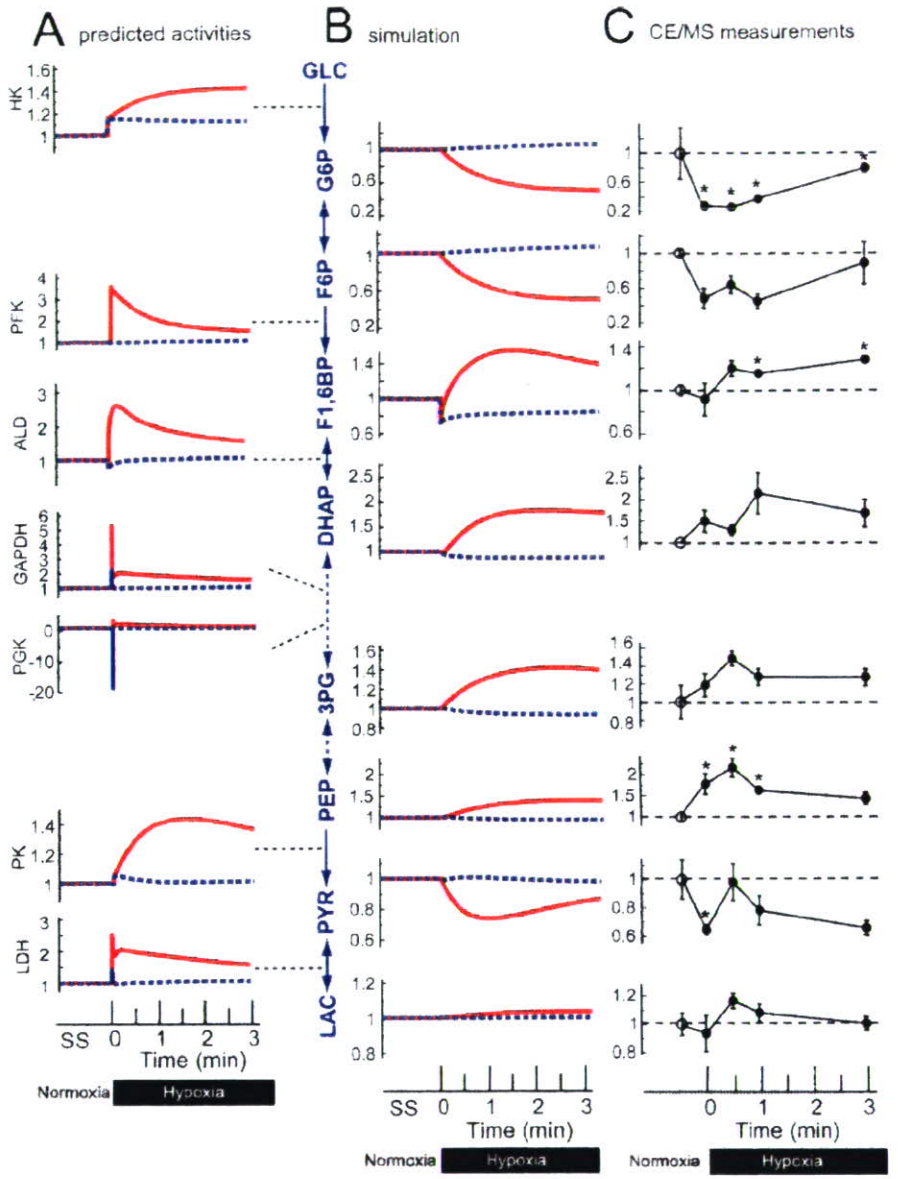

FIGURE 2. **Prediction of hypoxia-induced alterations in activities of glycolytic enzymes and in levels of their products in the mathematical model and demonstration by CE-MS analysis in human erythrocytes.** *A*, hypoxia-induced changes in predicted activities of glycolytic enzymes. *B*, predicted concentrations of glycolytic products. *Red* and *blue lines* indicate results of the simulation with and without inclusion of the BIII-Hb interactions, respectively. *C*, hypoxia-induced alterations in the relative concentrations of the products determined by CE-MS analysis. *Closed circles* indicate ratios of hypoxic metabolite concentrations to normoxic control concentrations, which are represented with *open circles*. Values are the mean ± S.E. of four separate experiments. *Asterisks*, $p < 0.05$ *versus* the steady-state base-line values.

Statistical Analyses—Differences in mean values among groups in the metabolome analyses were examined statistically using a one-way analysis of variance and Fisher's multiple comparison test.

RESULTS

Modeling the BIII-Hb Interaction Enhances Hypoxia-induced Activation of Glycolysis—Fig. 2*A* illustrates the differences in temporal alterations in the enzyme activities between the model involving BIII interactions with Hb and the glycolytic enzymes (BIII(+) model; *red solid line*) and the model without these interactions (BIII(−) model; *blue dotted line*) during the 3-min virtual hypoxia. Overall, the activities of glycolytic enzymes in the BIII(+) model were stimulated to greater extents than those in the BIII(−) model (Fig. 2*A*). The activity of HK, which mediates the initial reaction in glycolysis, was initially equally elevated upon hypoxia in the two models. Putative mechanisms for this increase will be mentioned under "Discussion." HK activity in the BIII(+) model exhibited further activation compared with the BIII(−) model; this difference appeared to result from a decrease in G6P (*uppermost panel* in Fig. 2*B*) and an increase in ATP, leading to a disappearance of HK product inhibition. Such an activation process is likely to help accelerate the initial step of glycolysis, as discussed below. As expected, the activities of PFK, ALD, and GAPDH, enzymes mediating the intermediate steps in glycolysis, modeled as BIII-binding enzymes, spiked immediately as a result of their release from BIII upon Hb binding. In contrast, the activity of these enzymes did not change greatly in the BIII(−) model, with the exception of GAPDH, which was elevated modestly but noticeably in the BIII(−) model. This elevation appeared to result from a decrease in 1,3-BPG, a product of the enzyme, through its binding to T-state Hb, as described in the model in supplemental Table 1. Other important differences to be noted in the BIII(+) model were the disappearance of the decreased activity of PGK and the marked activation of PK, whereas the activities of these ATP-generating enzymes were not predicted to contribute to acceleration of glycolysis in the BIII(−) model. The LDH activity was elevated in both models, but the elevation was substantially higher and sustained to a greater extent in the BIII(+) model compared with the BIII(−) model. As a result the temporal pattern of LDH activity in the BIII(+) model was similar to that of GAPDH. This behavior is due to the fact that NADH, a product of GAPDH, determines the activity of LDH. The predicted level of glycolytic metabolites indicated a unique profile in the BIII(+) model. In the BIII(−) model, G6P and F6P increased slightly, whereas F1,6BP, DHAP, 3PG. and PEP decreased modestly *versus* the steady-state base-line levels (Fig. 2*B*). In contrast, the BIII(+) model displayed a pattern opposite to the BIII(−) model, with

decreases in G6P and F6P by 50% and increases in F1,6BP, DHAP, 3PG, and PEP by 40% *versus* the corresponding baseline levels. The model predicted that pyruvate decreases, whereas lactate slightly increases in the BIII(+) model. The decrease in pyruvate seemed to result from a prediction by this model that consumption of pyruvate by LDH surpasses production by PK, as judged from the 2.5-fold peak increase in LDH activity *versus* the relatively modest activation of PK, which peaks at 1.4-fold. Because lactate is modeled to be transported according to a gradient between the intra- and extracellular spaces, elevation of lactate was small even in the BIII(+) model.

Demonstration of Hypoxia-induced Alterations in Glycolytic Products by CE-MS—The aforementioned results from the model raise the possibility that hypoxia-triggered activation of GAPDH drives activation of LDH as a downstream target through NADH generation and thereby facilitates the second half of the glycolytic reactions. Consequently, stimulation of the hypoxia-dependent BIII interaction of the intermediate enzymes (PFK, ALD, GAPDH) contributed to activation of HK as the initial step and that of PK and LDH as the final step in glycolysis in the model as a whole. To examine whether temporal alterations in the glycolytic metabolites of human erythrocytes occur in agreement with those predicted by the BIII(+)model, erythrocytes were exposed to hypoxia for 3 min, and the amounts of various metabolites were determined by CE-MS. As seen in Fig. 2*C*, G6P and F6P were significantly lower than those measured as steady-state controls under normoxic conditions. In contrast, levels of F1,6BP, DHAP, 3PG, and PEP were significantly greater than normoxic steady-state controls. These results are entirely consistent with those predicted by the BIII(+) model. The absolute concentrations of glycolytic metabolites measured by CE-MS at each time point are shown in supplemental Table 4.

Adsorption of 2,3-BPG and ATP to Hb during Protein Denaturation in Preparation for CE-MS—CE-MS validation of the data predicted by the dynamic mathematical model supported the hypothesis that hypoxia-dependent BIII interactions with PFK, GAPDH, and ALD play a crucial role in systematic activation of glycolytic reactions to support the demand for ATP in erythrocytes. As seen in Fig. 3*A*, the ATP content of the cells exposed to hypoxia at 4 °C was decreased by 30% *versus* that measured under normoxic steady-state conditions. This level of ATP was maintained and modestly elevated during the subsequent 3-min hypoxic conditions. Likewise, the content of 2,3-BPG did not decrease in hypoxia but, rather, was elevated during the 3-min hypoxic period. Because these metabolites are known to adsorbed by T-state Hb, we examined whether the current protocol for measuring metabolites reflected only the amount of free metabolite (*i.e.* that not bound to Hb) or the total amount in the cells. As seen in Fig. 3*B*, the presence of free T-state Hb, stabilized by dithionite, but not free R-state Hb, stabilized under normoxia without dithionite, caused apparent decreases in ATP and 2,3-BPG contents but not in G6P, lactate, and 2-oxoglutarate contents. Approximately 30% of the ATP and 90% of the 2,3-BPG were lost during the protein denaturation step before CE-MS.

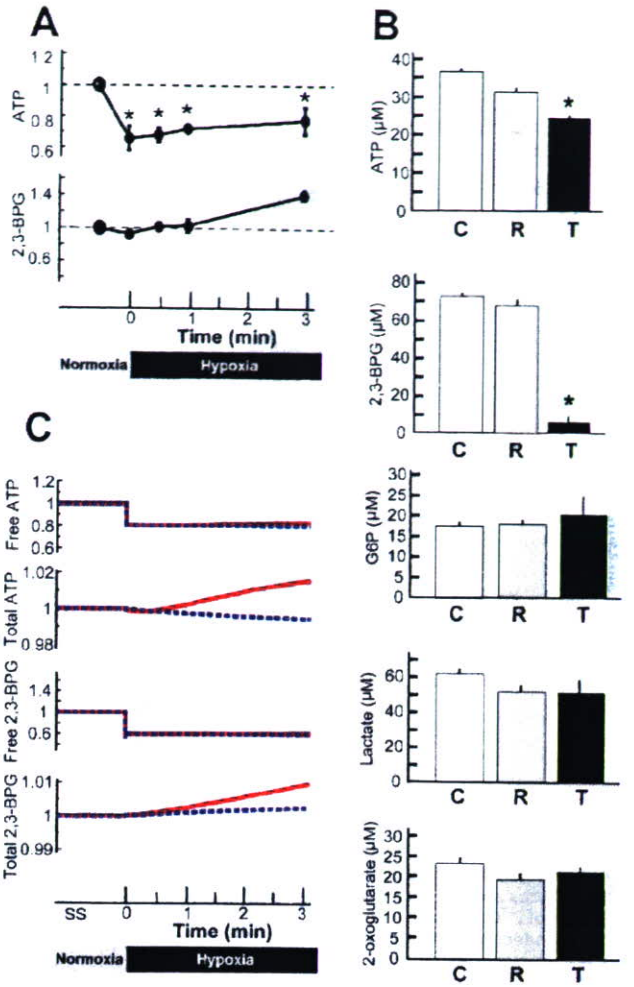

FIGURE 3. **Hypoxia-induced alterations in measured concentrations of ATP and 2,3-BPG and effects of the presence of Hb on measurements of metabolites by CE-MS.** *Panel A*, hypoxia-induced changes in measured concentration of ATP and 2,3-BPG. *Panel B*, influence of the presence of Hb. *C*, standard measurements in the Hb-free buffer; *R* and *T*, measurements in Hb-containing buffer under ambient and hypoxic conditions, respectively. Data shown are the means ± S.D. of three separate experiments. *, $p < 0.05$ *versus* the R group. *Panel C*, prediction indicating temporal alterations in free and total ATP and 2,3-BPG in the model. *Red lines*, data collected from the BIII(+) model. *Blue dotted lines*, data collected from the BIII(−) model.

These results suggest that in the cell-free protein solution the ATP and 2,3-BPG data obtained from CE-MS could be underestimated because CE-MS only takes into account free metabolite contents and neglects the Hb-bound forms of these metabolites. On the other hand in the case of the cell-containing system, the T-state of Hb in the hypoxia-exposed erythrocytes could be easily stabilized into the R-state (35) during centrifugation at low temperatures before protein denaturation; such a process before sample processing could stimulate the release of 2,3-BPG adsorbed to Hb under hypoxic conditions. Considering the above, we compared the CE-MS data for ATP and 2,3-BPG with the predicted data for free and total amounts of these metabolites obtained from the model. As seen in Fig. 3*C*, the temporal profile of free ATP in the model was in good agreement with the CE-MS results for ATP shown in Fig. 3*A*. The amounts of

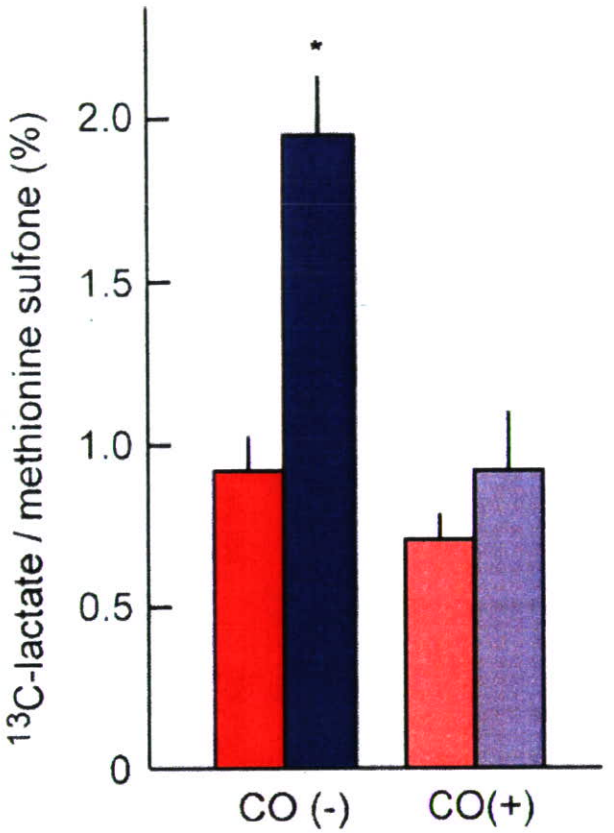

FIGURE 4. **Hypoxia-induced acceleration of glycolysis assessed by pulse-chase analysis of the conversion of [^{13}C]glucose to [^{13}C]lactate in human erythrocytes and its blockade by CO.** *Red* and *blue bars* indicate relative amounts of [^{13}C]lactate generated per 1 min after loading with [^{13}C]glucose at 5 mM under normoxic and hypoxic conditions, respectively. *CO(−)*, control erythrocytes not treated with CO. *CO(+)*, CO-pretreated erythrocytes. Methionine sulfone is an internal standard that was added at 100 μM to protein-free samples for CE-MS collected from the erythrocyte lysates. Means ± S.E. of 3–4 separate experiments are shown. *, $p < 0.05$ *versus* normoxic controls (CO(−)).

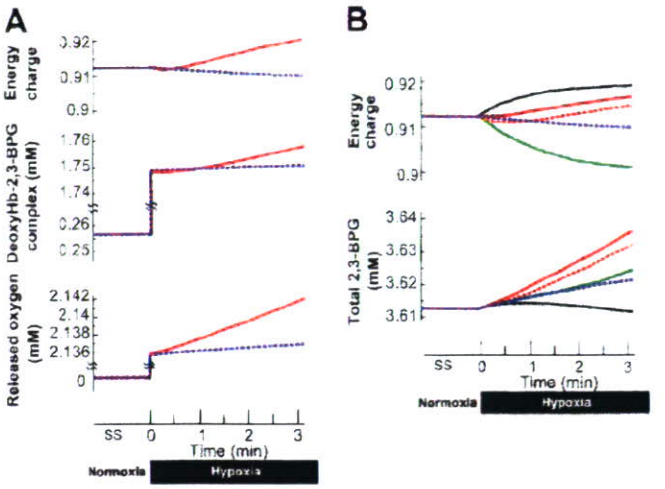

FIGURE 5. **Beneficial effects of BIII-Hb interactions on cellular energetics and Hb allostery predicted by the mathematical model.** *A*, hypoxia-induced alterations in the values of energy charge which is defined by (ATP + 0.5ADP)/(AMP + ADP + ATP). *B*, the sensitivity analysis indicating changes in energy charge (*upper*) and 2,3-BPG (*lower*) generation under different hypoxic conditions when the amounts of the following enzymes were increased by 2-fold: PFK + ALD + GAPDH (*red*), none (same as BIII(−) model) (*blue*), HK (*green*), PFK (*broken red*), and PK (*black*). Note that HK activation results in a decrease in energy charge and an increase in 2,3-BPG generation, whereas PK activation alone increases energy charge without stimulating 2,3-BPG generation, suggesting that activation of PFK or PFK + ALD + GAPDH leads to simultaneous increases in energy charge and 2,3-BPG generation in the model.

total ATP in the model were modestly elevated. On the other hand the prediction of the temporal profile of free 2,3-BPG, whose adsorption is dictated by the T-state of Hb, displayed an abrupt drop compared with the steady-state base-line value. This difference with respect to the CE-MS data (Fig. 3*A*) is not surprising when the aforementioned effect of low temperature on 2,3-BPG release from the T-state of Hb is taken into consideration. In the model prediction the amount of total 2,3-BPG gradually increased with time, suggesting that the drop in free 2,3-BPG predicted in the model does not result from down-regulation of its synthesis but from its adsorption to Hb. This was demonstrated by the [$^{13}C_6$]glucose pulse-chase measurements described below.

Hypoxia Induces Acceleration of Glycolysis in Human Erythrocytes—The results of the metabolome analyses (Figs. 2 and 3) suggest that hypoxia causes activation of glycolysis. To examine whether the actual flux of glycolysis could be accelerated in response to hypoxia, we determined the rate of conversion of [^{13}C]glucose into [^{13}C]lactate in human erythrocytes. As seen in Fig. 4, the rate of production of [^{13}C]lactate was accelerated 1.8-fold within 1 min after exposure to hypoxia. In contrast, pretreatment of the cells with CO to stabilize Hb in the R-state attenuated the hypoxia-induced acceleration of lactate production almost completely. These results suggest that the hypoxia-induced stabilization of T-state Hb plays a crucial role in triggering glycolytic activation in erythrocytes.

The Model Including BIII-Hb Interaction Predicts Sustained Energy Charge and Accelerated O_2 Release—Using the dynamic mathematical model validated by CE-MS analysis, we examined the roles of the BIII-Hb interaction in regulation of cellular energetics and O_2 delivery. As an index of the content of high energy phosphate bonds of adenylate nucleotides, an energy charge was calculated for the BIII(+) and BIII(−) models. As seen in the *upper panel* of Fig. 5*A*, the basal energy charge under normoxic steady-state conditions was 0.91. This value, obtained by the model prediction, was comparable with that reported in previous studies ranging from 0.86 (36) to 0.935 (37), supporting the hypothesis that the BIII(+) model is consistent with the real metabolic behavior of human erythrocytes. Upon exposure to hypoxia, the BIII(+) model exhibited further increases in the energy charge and in the amounts of the deoxy-Hb-2,3-BPG complex (Fig. 5*A*). Under these circumstances the amounts of O_2 released from the cell is greater in the BIII(+) model than in the BIII(−) model.

Based on the predictions of the mathematical model shown in Fig. 5*A* as well as in Fig. 3*C*, we also examined differences in the conversion of glucose to 2,3-BPG between normoxic and hypoxic cells under the same experimental conditions as in Fig. 4. The ratios of [$^{13}C_3$]2,3-BPG/methionine sulfone were 2.1 ± 0.3 and 5.4 ± 0.2% (mean ± S.E. of 1-min incubations in 4 separate experiments) under nor-

moxic and hypoxic conditions, respectively, indicating a significant acceleration in *de novo* 2,3-BPG synthesis upon hypoxia. Considering the CE-MS data in Fig. 3*A*, indicating maintenance of free 2,3-BPG in erythrocytes, the results achieved by the model were consistent with the hypothesis that the BIII-Hb interaction contributes greatly to the delivery of 2,3-BPG to Hb to stabilize the T-state and, thereby, to sustain the release of O_2 in hypoxic conditions.

In Fig. 5*B*, we conducted sensitivity analysis to determine whether or not the amount of any particular enzyme making up the glycolytic pathway could alter the effectiveness of the sustained increase in energy charge and 2,3-BPG generation during hypoxia in the model. We, therefore, increased the amount of each glycolytic enzyme in the pathway by 2-fold simultaneously with hypoxia. As shown in Fig. 5*B*, HK activation (*green line* in *panel B*) resulted in a decrease in energy charge and an increase in 2,3-BPG, whereas PK activation (*black* in *panel B*) increased energy charge without stimulating 2,3-BPG generation. On the other hand, activation of PFK (*broken red* in *panel B*) or PFK+ALD+GAPDH (*red* in *panel B*) led to simultaneous elevation of energy charge and 2,3-BPG generation in the model. These analyses suggest that activation of enzymes situated midway through the glycolytic pathway positively regulate energy charge and 2,3-BPG generation simultaneously in erythrocytes. The results lend further support to the notion that sustained elevation of 2,3-BPG and the resultant increase in O_2 release predicted by the model are likely to be metabolically relevant.

DISCUSSION

Glycolysis involves a series of enzymatic reactions to couple glucose oxidation to generation of ATP. On the basis of previous studies (for metabolism (21, 24) and for BIII-enzymes/Hb interactions (13, 14)), the BIII(+) model simulated dynamic alterations in enzyme activities and the corresponding metabolites using the assumption that the intermediate glycolytic enzymes, such as PFK, GAPDH, and ALD, bind to R-state Hb in their quiescent form and become activated upon their release from T-state Hb in response to hypoxia. The model predictions developed in this study clearly indicate that such an activation of the intermediate enzymes triggered by hypoxia-induced stabilization of T-state Hb not only induces acceleration of the flux of metabolites through the glycolytic reactions but also triggers activation of the initial and final steps of glycolysis as a result of alterations in the corresponding allosteric effectors (*e.g.* 2,3-BPG for HK) and levels of substrates and products (*e.g.* ATP and G6P for HK, NADPH for LDH).

As a consequence, PGK and PK, the glycolytic enzymes for ATP synthesis, are predicted to be accelerated upon hypoxia. The predicted hypoxia-induced remodeling of glycolytic enzyme activities results in decreases in upstream products such as G6P and F6P and increases in the intermediate products such as F1,6BP, DHAP, 3PG, 2,3-BPG, and PEP. Furthermore, these predicted alterations in glycolytic products were actually demonstrated by CE-MS analysis in human erythrocytes. These results indicate that the mathematical model described in this study is capable of predicting hypoxia-induced remodeling of energy metabolism, suggesting a physiological significance of the BIII-Hb interaction in accelerating glycolysis in erythrocytes upon exposure to hypoxia.

The sensitivity analysis, showing that the activation of these glycolytic enzymes altered hypoxia-induced responses of metabolites, led us to suggest that the alterations in metabolites determined by CE-MS are comparable with those elicited by about a 2–5-fold increase in the amounts of PFK (supplemental Fig. 1*A*). On the other hand the increases in ALD and GAPDH apparently had little or no effect on glycolytic activation. However, careful analysis of the sensitivity data (supplemental Fig. 1, *A–C*) indicates that increases in the latter two enzymes obviously contributed to the spike in the activation of LDH. It is worthwhile noting that such an initial LDH spike is observed in Fig. 2*A* but not in supplemental Fig. 1*A*, where only PFK is activated. Thus, these simulations collectively suggest that PFK activation plays a major role, whereas activation of ALD and/or GAPDH *per se* plays a minimal role. This does not exclude, however, a cooperative effect of these two latter enzymes in PFK activation for the stimulation of downstream reactions in the glycolytic pathway, which may be of physiologic and metabolic importance.

Our results show the predicted time-dependent alterations in concentrations of metabolites and the demonstration by CE-MS of these changes. The changes are physiologically relevant to previous observations of hypoxia-elicited metabolic responses in human erythrocytes. For instance, the change in G6P could not only influence glycolysis but also regulate other metabolic pathways. In the BIII(+) model, but not in the BIII(−) model, G6P decreased rapidly after the onset of hypoxia. Because this metabolite serves as a substrate for G6PDH, the rate-limiting step of the pentose phosphate pathway, such a change in G6P could rapidly limit the flux of metabolites through this pathway. We were unable to detect a decrease in the flux of [^{13}C]glucuronolactone, the product of G6PDH, presumably because the changes were insufficient to be detected by CE-MS. However, the hypothesis is well supported by previous observations that hypoxia causes down-regulation of the pentose phosphate pathway, in parallel with an acceleration in glycolysis in erythrocytes (38). Second, erythrocytes exposed to hypoxia have been known to release ATP into the extracellular space, which results in endothelium-dependent vasorelaxation of arterioles (3, 39, 41). Considering that the K_m of the purinergic receptor for ATP is in the submicromolar range, the amount of ATP released from erythrocytes appears to be far smaller than levels normally found in the intracellular spaces. Despite the fact that the time needed to transit through the organ microvascular systems is thought to be in the range of several seconds, erythrocytes could undergo hypoxia frequently during their passage through the capillaries. In some organs (*e.g.* liver) erythrocytes exhibit transitory stasis among the capillary networks (42, 43). Under these circumstances glycolytic acceleration triggered by the BIII-Hb interaction could greatly enhance the maintenance of intracellular ATP levels.

In this context acceleration of glucose oxidation upon exposure to hypoxia is likely to be necessary to maintain the functional integrity of erythrocytes through at least two different aspects; that is, supplementation of ATP and sustained stabilization of T-state Hb by 2,3-BPG, an allosteric effector generated through a side reaction in glycolysis. Judging from the CE-MS measurements shown in Fig. 3*A*, the free amounts of ATP and 2,3-BPG were not apparently reduced during the 3-min hypoxia. Considering that deoxy-Hb has a greater ability to absorb these metabolites than oxy-Hb, these results led us to hypothesize that *de novo* synthesis of these metabolites is dramatically up-regulated during even short periods of hypoxia. Evidence to support this hypothesis was well documented by the CE-MS measurements, indicating accelerated conversion of ^{13}C-labeled glucose into 2,3-BPG and lactate under hypoxic conditions. As predicted by the mathematical model in Fig. 5*A*, such an acceleration of 2,3-BPG synthesis is likely to contribute to a rapid increase in the Hb-2,3-BPG complex that could consequently lead to the release of residual Hb-bound O_2 from erythrocytes.

Through further analyses of the model depicted in Fig. 5*B*, we suggest that PFK activation is a crucial step for the up-regulation of both energy charge and 2,3-BPG generation, whereas activation of the initial (*e.g.* HK) or final (*e.g.* PK) steps of the glycolytic pathway fails to satisfy these requirements. Furthermore, activation of ALD or GAPDH with that of PFK appears to help activate LDH at the onset of hypoxia. Whether the amounts of O_2 released from the cells through these putative mechanisms are sufficient to fulfill tissue O_2 demand should be further examined *in vivo*.

In this model several of the components of real erythrocytes are missing. For instance, hypoxia-induced switching between BIII and three glycolytic enzymes is simply based on their individual association constants for binding to BIII. On the other hand, a previous report suggested that these enzymes behave as a macromolecular complex for the execution of glycolysis (13). Because pH effects on Hb allostery were not included in the current model, the disparity in O_2 saturation between BIII(+) and BIII(−) models could in reality be greater than that calculated in this study. In addition, the initial environmental conditions governing external metabolite concentrations (*e.g.* lactate in the extracellular space) could be altered under disease conditions. Such an alteration, however, did not change the prediction of hypoxia-induced glycolytic remodeling *in silico* (supplemental Fig. 2). With regard for these considerations, the model needs to be further refined by including the function of carbonic anhydrase, an enzyme that senses tissue CO_2 (6). This would be very helpful when it comes to applying the current model for the prediction of time-dependent alterations in erythrocyte metabolism under chronically hypoxic conditions.

REFERENCES

1. Murphy, J. R. (1960) *J. Lab. Clin. Med.* **55,** 286–302
2. Lenfant, C., Torrance, J., English, E., Finch, C. A., Reynafarje, C., Ramos, J., and Faura, J. (1968) *J. Clin. Investig.* **47,** 2652–2656
3. Ellsworth, M. L., Forrester, T., Ellis, C. G., and Dietrich, H. H. (1995) *Am. J. Physiol.* **269,** H2155–H2161
4. Bergfeld, G. R., and Forrester, T. (1992) *Cardiovasc. Res.* **26,** 40–47
5. Jagger, J. E., Bateman, R. M., Ellsworth, M. L., and Ellis, C. G. (2001) *Am. J. Physiol. Heart Circ. Physiol.* **280,** 2833–2839
6. Jensen, F. B. (2004) *Acta Physiol. Scand.* **182,** 215–227
7. Southgate, C. D., Chishti, A. H., Mitchell, B., Yi, S. J., and Palek, J. (1996) *Nat. Genet.* **14,** 227–230
8. Tsuneshige, A., Imai, K., and Tyuma, I. (1987) *J. Biochem. (Tokyo)* **101,** 695–704
9. Higashi, T., Richards, C. S., and Uyeda, K. (1979) *J. Biol. Chem.* **254,** 9542–9550
10. Murthy, S. N., Liu, T., Kaul, R. K., Kohler, H., and Steck, T. L. (1981) *J. Biol. Chem.* **256,** 11203–11208
11. Kliman, H. J., and Steck, T. L. (1980) *J. Biol. Chem.* **255,** 6314–6321
12. Harris, S. J., and Winzor, D. J. (1990) *Biochim. Biophys. Acta* **1038,** 306–314
13. Campanella, M. E., Chu, H., and Low, P. S. (2005) *Proc. Natl. Acad. Sci. U. S. A.* **102,** 2402–2407
14. Chu, H., and Low, P. S. (2006) *Biochem. J.* **400,** 143–151
15. Costa, L. E., and De Miranda, I. M. (1976) *Acta Physiol. Latinoam.* **26,** 115–121
16. Moore, L. G., and Brewer, G. J. (1980) *Am. J. Phys. Anthropol.* **53,** 11–18
17. Rapoport, T. A., and Heinrich, R. (1975) *Biosystems* **7,** 120–129
18. Rapoport, T. A., Heinrich, R., and Rapoport, S. M. (1976) *Biochem. J.* **154,** 449–469
19. Joshi, A., and Palsson, B. O. (1989) *J. Theor. Biol.* **141,** 515–528
20. Joshi, A., and Palsson, B. O. (1989) *J. Theor. Biol.* **141,** 529–545
21. Joshi, A., and Palsson, B. O. (1990) *J. Theor. Biol.* **142,** 41–68
22. Joshi, A., and Palsson, B. O. (1990) *J. Theor. Biol.* **142,** 69–85
23. Mulquiney, P. J., Bubb, W. A., and Kuchel, P. W. (1999) *Biochem. J.* **342,** 567–580
24. Mulquiney, P. J., and Kuchel, P. W. (1999) *Biochem. J.* **342,** 581–596
25. Soga, T., Baran, R., Suematsu, M., Ueno, Y., Ikeda, S., Sakurakawa, T., Kakazu, Y., Ishikawa, T., Robert, M., Nishioka, T., and Tomita, M. (2006) *J. Biol. Chem.* **281,** 16768–16776
26. Soga, T., Ohashi, Y., Ueno, Y., Naraoka, H., Tomita, M., and Nishioka, T. (2003) *J. Proteome Res.* **2,** 488–494
27. Tomita, M., Hashimoto, K., Takahashi, K., Shimizu, T. S., Matsuzaki, Y., Miyoshi, F., Saito, K., Tanida, S., Yugi, K., Venter, J. C., and Hutchison, C. A., III (1999) *Bioinformatics* **15,** 72–84
28. Takahashi, K., Yugi, K., Hashimoto, K., Yamada, Y., Pickett, C., and Tomita, M. (2002) *IEEE Intell. Syst.* **17,** 64–71
29. Dash, R. K., and Bassingthwaighte, J. B. (2004) *Ann. Biomed. Eng.* **32,** 1676–1693
30. Tsai, A. G., Johnson, P. C., and Intaglietta, M. (2003) *Physiol. Rev.* **83,** 933–963
31. Suganuma, K., Tsukada, K., Kashiba, M., Tsuneshige, A., Furukawa, T., Kubota, T., Goda, N., Kitajima, M., Yonetani, T., and Suematsu, M. (2006) *Antioxid. Redox Signal.* **8,** 1847–1855
32. Soga, T., Ueno, Y., Naraoka, H., Ohashi, Y., Tomita, M., and Nishioka, T. (2002) *Anal. Chem.* **74,** 2233–2239
33. Atkinson, D. E. (1968) *Biochemistry* **7,** 4030–4034
34. Atkinson, D. E., and Walton, G. M. (1967) *J. Biol. Chem.* **242,** 3239–3241
35. Yonetani, T., Tsuneshige, A., Zhou, Y., and Chen, X. (1998) *J. Biol. Chem.* **273,** 20323–20333
36. Komarova, S. V., Mosharov, E. V., Vitvitsky, V. M., and Ataullakhanov, F. I. (1999) *Blood Cells Mol. Dis.* **25,** 170–179
37. Shimizu, T., Kono, N., Kiyokawa, H., Yamada, Y., Hara, N., Mineo, I., Kawachi, M., Nakajima, H., Wang, Y. L., and Tarui, S. (1988) *Blood* **71,** 1130–1134
38. Messana, I., Orlando, M., Cassiano, L., Pennacchietti, L., Zuppi, C., Castagnola, M., and Giardina, B. (1996) *FEBS Lett.* **390,** 25–28
39. Sprague, R. S., Ellsworth, M. L., Stephenson, A. H., and Lonigro, A. J. (1996) *Am. J. Physiol.* **271,** H2717–H2722
40. von Ruckmann, B., and Schubert, D. (2002) *Biochim. Biophys. Acta* **1559,** 43–55
41. Ellsworth, M. L. (2004) *Med. Sci. Sports Exerc.* **36,** 35–41
42. MacPhee, P. J., Schmidt, E. E., and Groom, A. C. (1995) *Am. J. Physiol.* **269,** G692–G698
43. Hauck, E. F., Apostel, S., Hoffmann, J. F., Heimann, A., and Kempski, O. (2004) *J. Cereb. Blood Flow Metab.* **24,** 383–391

44. Qian, H., and Beard, D. A. (2005) *Biophys. Chem.* **114,** 213–220
45. Magnani, M., Stocchi, V., Piatti, E., Dacha, M., Dallapiccola, B., and Fornaini, G. (1983) *Blood* **61,** 915–919
46. Yamamoto, T., Moriwaki, Y., Takahashi, S., Ishizashi, H., and Higashino, K. (1994) *Horm. Metab. Res.* **26,** 504–508
47. Mills, G. C., Schmalstieg, F. C., Trimmer, K. B., Goldman, A. S., and Goldblum, R. M. (1976) *Proc. Natl. Acad. Sci. U. S. A.* **73,** 2867–2871
48. Walder, J. A., Chatterjee, R., Steck, T. L., Low, P. S., Musso, G. F., Kaiser, E. T., Rogers, P. H., and Arnone, A. (1984) *J. Biol. Chem.* **259,** 10238–10246
49. Jenkins, J. D., Madden, D. P., and Steck, T. L. (1984) *J. Biol. Chem.* **259,** 9374–9378

Current Eye Research, 32:83–88, 2007

ISSN: 0271-3683 print / 1460-2202 online
DOI: 10.1080/02713680601147690

informa
healthcare

Albumin Rescues Ocular Epithelial Cells from Cell Death in Dry Eye

Akihiro Higuchi
Department of Ophthalmology, Keio University School of Medicine, Tokyo, Japan

Ryuji Ueno
Sucampo AG, Zug, Swizterland

Shigeto Shimmura
Department of Ophthalmology, Keio University School of Medicine, Tokyo, Japan

Makoto Suematsu
Department of Biochemistry and Integrative Medical Biology, Keio University School of Medicine, Tokyo, Japan

Murat Dogru and Kazuo Tsubota
Department of Ophthalmology, Keio University School of Medicine, Tokyo, Japan

ABSTRACT *Purpose*: Because autologous serum is useful for the treatment of severe dry eye, serum components may be a potential candidate for the treatment of dry eye. Serum albumin is abundantly contained in human serum and plays many physiologic roles. We investigated the efficacy of serum albumin in a dry eye animal model. *Methods*: Sprague-Dawley rats were used to make dry eye model rats according to a previous study. The central region of the corneal epithelium was scraped mechanically, and the rats were placed in a desiccation room (temperature, 23 ± 2°C; humidity, 28 ± 2%; air flow, 2–4 m/s) for 12 hr. During desiccation, one eye of each rat was treated with human serum albumin eye drops, and the other eye was given a drop of phosphate buffered saline (PBS). Human corneal and conjunctival cell lines were used to investigate suppression effect of albumin on apoptosis induced by addition of apoptosis inducers or serum deprivation, respectively. *Results*: The erosion area was increased by 12 hr of desiccation. Albumin treatment decreased the area of erosion compared with PBS treatment. Apoptosis suppression assay using cell lines revealed that caspase-3 activation induced by serum deprivation and DNA fragmentation induced by addition of apoptosis inducers were dose-dependently suppressed by albumin. *Conclusions*: Albumin showed a therapeutic effect in dry eye model rats. This efficacy may be related to the suppression of apoptosis by albumin.

KEYWORDS albumin; apoptosis; conjunctiva; cornea; dry eye

INTRODUCTION

Severe dry eye results not only from dryness of the ocular surface but also from the lack of tear components, which are essential for maintaining the ocular surface.[1–5] Artificial tears are useful for the treatment of dry eye, but the efficiency of the components included in artificial tears is not comparable with that of human tears. In a previous study, we used autologous serum as a substitute for tears for the treatment of severe dry eye and observed dramatic improvement of the ocular surface.[6] The efficient therapeutic effects of serum in cases of severe dry eye also suggest that the components of serum that are essential for maintaining a viable ocular surface may be the same or similar to those of tears.[7] A comparative analysis revealed that serum components were similar to tear components.[8]

Received 9 June 2006
Accepted 29 November 2006
Correspondence: Akihiro Higuchi, Ph.D., 6N9 Research Park, Keio University, School of Medicine, 35 Shinano-machi, Shinjyuku-ku, Tokyo 160-8582, Japan.
E-mail: ahiguchi@sc.itc.keio.ac.jp

Human serum albumin (HSA) is monomeric single-chain protein synthesized and secreted by liver cells. HSA is constituted from 585 amino acids and does not have any prosthetic groups.[9,10] Its molecular weight is 66.5 kDa, and the ratio of HSA in serum proteins is approximately 50%.[8] Because HSA is a remarkably stable protein, it is distributed widely in body fluids. Many techniques used to investigate protein composition of human tears[11–13] revealed that HSA was also distributed in tears, where the ratio of albumin in tears was approximately 1%.[8]

In our previous study, we used 50 mg/ml albumin as eye drops for patients with Sjögren syndrome with severe dry eye.[14] The patients showed significant improvement in fluorescein and rose bengal scores, but not in tear break-up time and subjective symptoms. In this study, we investigate the effect of albumin as artificial tears for dry eye *in vivo* and *in vitro*.

MATERIALS AND METHODS

Animals

Male 8-week-old Sprague-Dawley rats (n = 12 in each experiment) were purchased from Tokyo Laboratory Animal Science Co., Ltd. (Tokyo, Japan). They were quarantined and acclimatized before the experiments for a 1-week period under standard conditions: room temperature 23 ± 2°C, relative humidity 60 ± 10%, an alternating 12-hr light-dark cycle (8 am. to 8 pm.), with water and food available *ad libitum*. All procedures were performed according to the ARVO Statement for the Use of Animals in Ophthalmic and Vision Research.

Dry Eye Model Rat

The dry eye model rat experiment was performed according to a previous study.[15] The rats were anesthetized by intramuscular injection of an anesthesia cocktail, and the central region of the corneal epithelium (0.4 mm^2) was scraped mechanically with an ophthalmic surgical blade. After scraping, the rats were placed in a desiccation room, with room temperature of 23 ± 2°C, relative humidity of 28% ± 2%, and constant air flow (2–4 m/s), and maintained for 12 hr. During desiccation, one eye of each rat was treated with HSA (Wako Pure Chemical Industries, Ltd., Osaka, Japan) dissolved in PBS and the other eye was given a drop of PBS as the control. The concentration of HSA was 1, 5, and 10 mg/ml, respectively. The range of HSA concentration in eye drop was based on the following reasons: In a previous study, we used autologus diluted serum (20% serum) as a substitute for tears for the treatment of dry eye.[7] The concentration of albumin in diluted serum is approximately 7 to 11 mg/ml. Ten microliters of eye drops was administered every hour for 12 hr.

The damaged areas were photographed immediately and 12 hr after scraping by applying a fluorescein solution under cobalt-blue light. The stained area (epithelial erosion) was digitized with an optical scanner and quantified with image-analysis software (NIH Image, distributed by Wayne Rasband, National Institutes of Health, Bethesda, MD, USA).

Apoptosis Assay

Human conjunctival cell line CCL-20.2 (CCL) was obtained from the American Type Culture Collection (Manassas, VA, USA). The cells were grown to 70–80% confluence in 75-cm^2 flasks with Medium 199 (Gibco BRL Life Technologies, Rockville, MD, USA) containing 10% fetal calf serum (FCS; Gibco BRL Life Technologies). The medium was removed, and cells were cultured for 24 hr in serum- free Medium 199 with or without HSA. The cells were harvested and solubilized with 50 mM HEPES buffer (pH 7.4) containing 0.1% {3-[(3-Cholamidopropyl)-dimethylammonio}-1-propanesulfonate (CHAPS), 0.1 mM phenylmethanesulfonyl fluoride (PMSF), 1 mM dithiothreitol (DTT), and 0.1 mM ethylenediaminetetraacetic acid (EDTA) for 5 min in an ice bath. They were then centrifuged at 10,000 × *g* for 10 min at 4°C to obtain the supernatants. The caspase activities of cell extracts were measured using artificial fluorescent substrates (DEVD-AFC; Enzyme System Products, Livermore, CA, USA) with a fluorescent microplate reader (ARVO SX; PerkinElmer Life Sciences Japan Co., Ltd., Tokyo, Japan).[16]

Cell extracts were mixed with 50 mM HEPES buffer (pH 7.4) containing 100 mM NaCl, 0.1% CHAPS, 10 mM DTT, 0.1 mM EDTA, and 10% glycerol in 96-well plate. Enzyme reaction was started by addition of 0.1 mM artificial substrate to well. Fluorescence was measured immediately and after incubation for 1 hr at 37°C (excitation wavelength, 400 nm; emission wavelength, 505 nm).

Human corneal epithelial cell line CEPI-17-CL4 (CEPI) was kindly provided by Dr. Kuwahara (Alcon Laboratories, Fort Worth, TX, USA). These cells were immortalized by infection with a recombinant SV40-retrovirus vector containing the BglI-HpaI fragment of SV40 T-antigen[17] and express an extensive array of

cytokines, growth factors, and metabolic enzymes that resemble the original tissue.[18] CEPI was cultured to 70–80% confluence in 96-well plate with keratinocyte basal medium 2 (KBM-2; Clonetics Corp., San Diego, CA, USA). The cells were treated with apoptosis inducers (anti-Fas antibody and etoposide) in the presence or absence of 5 mg/ml HSA. DNA fragmentation was measured by using Cell Death Detection ELISA (Roche Diagnostics Corporation, Indianapolis, IN, USA). This assay was conducted according to the manufacturer's protocol. Briefly, DNA fragments were bound to peroxidase-labeled anti-DNA antibody, and the production of antibody-DNA fragment complex was measured photometrically using 2,2′-Azinobis(3-ethylbenzothiazolin-6-sulfonate) (ABTS) as the substrate.

RESULTS

Dry Eye Model Rat

The fluorescein-staining area in Figure 1A was a scraped area. In the control group, the scraped region of the corneal epithelium gradually diminished and disappeared within 12 hr.[15] In the dry eye group, the scraped region was clearly aggravated after 12 hr in the desiccation chamber (Fig. 1B).

To investigate the effect of HSA on corneal epithelial defects induced by desiccation, clinical observations were done after 12 hr of desiccation. HSA treatment decreased the area (Fig. 1C), whereas PBS treatment only had a mild effect (Fig. 1D) compared with no treatment. The effect of HSA is shown in Figure 2. Albumin eye drop decreased the fluorescein-stained areas. Significant decreases in the fluorescein-stained areas were observed in the 5 mg/ml eye drop group compared with PBS control ($p < 0.01$).

Apoptosis Assay

It was shown that apoptosis was induced in the conjunctiva[19] and corneal epithelium[20] in dry eye, although the mechanism involved is still unclear. Previously, our study showed that aggravation of the scraped

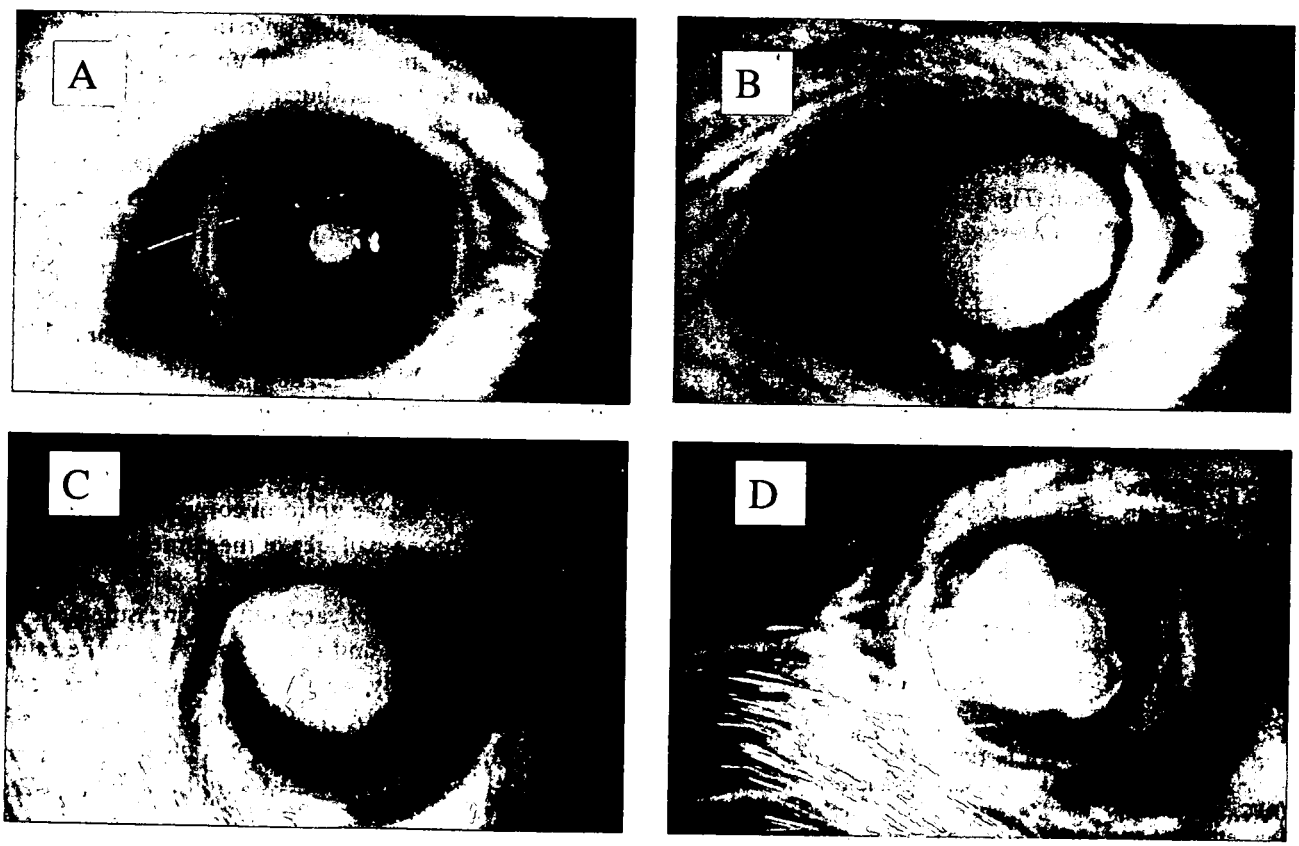

FIGURE 1 Fluorescein staining of corneal epithelial erosion induced by ocular surface desiccation. The damaged areas were photographed by applying fluorescein solution under cobalt-blue light. (A) Zero hours after scraping; (B) 12 hr after scraping with no treatment; (C) 12 hr after scraping with 5 mg/ml HSA treatment; (D) 12 hr after scraping with PBS treatment.

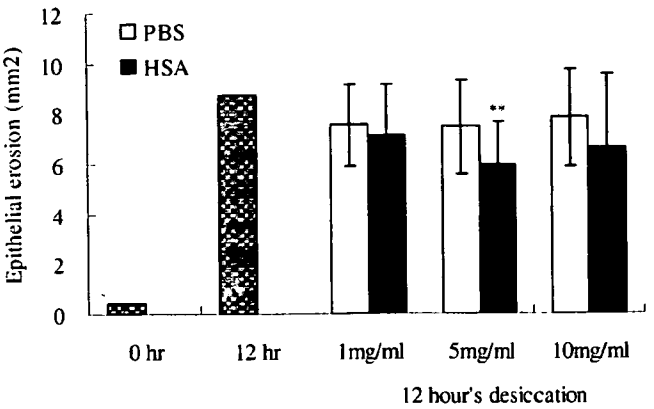

FIGURE 2 The size of epithelial erosion before treatment, without treatment, and after treatment with three different concentrations of albumin. HSA (1, 5, and 10 mg/ml) was applied at 1-hr intervals during ocular surface desiccation. After 12 hr, quantitative analysis of the fluorescein-stained area of the corneal epithelium was performed on each eye. [0 hr and 12 hr means 0 hr after scraping and 12 hr after scraping (n = 1) with no treatment in a desiccation room, respectively.] The scraped area at 0 hr is fixed (0.4 mm^2). Data of HSA or PBS eye drops represent the mean ± SD of 12 experiments. Paired Student's *t* test was used to determine the significance of differences. **Indicates a significant difference from the result in PBS treatment, $p < 0.01$.

region in cornea epithelial of rats caused by placement in a desiccation room was involved in apoptosis demonstrated by Hoechst 33342 staining.[15] It is also known that CCL does not survive when serum is removed from the medium. This cell death was apoptosis accompanied by caspases activation (Fig. 3). Figure 3 shows that HSA dose-dependently suppressed apoptosis.

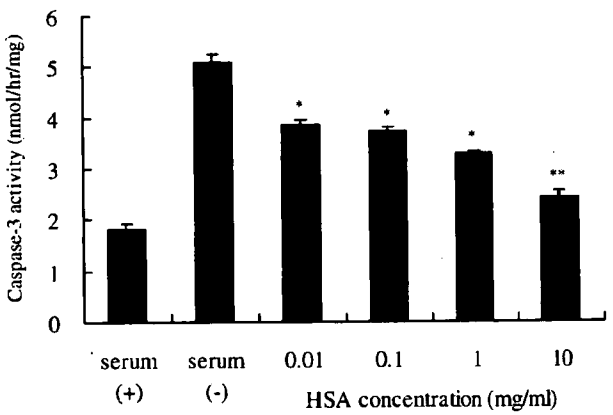

FIGURE 3 Suppression of caspase-3 activation induced by serum deprivation by HSA in CCL. Activity of caspase-3 was estimated by measuring the 7-amino-4-trifluoromethyl coumarin (AFC) production. Results are the mean ± SD (n = 4). Dunnett's test was used to determine the significance of differences. *Indicates a significant difference from the result in serum (−), which is incubated in serum-free Medium 199 without HSA. $p < 0.05$. **Indicates a significant difference from the result in serum (−), $p < 0.01$.

Furthermore, suppression effect of HSA on apoptosis induced by apoptosis inducers in corneal epithelial cells was investigated. It was demonstrated in many studies that the activation of caspase correlated with DNA fragmentation. DNA fragmentation of CEPI was dose-dependently induced by anti-Fas antibody (Fig. 4A) or etoposide (Fig. 4B), and this fragmentation was suppressed by 0.5 mg/ml albumin.

DISCUSSION

In this and previous studies from our group,[14] we have shown that HSA has potential for clinical treatment of dry eye patients. Because autologous serum is a good substitute for tears, we hypothesized that common components between serum and tears may be effective for treatment of dry eye. Serum albumin, which is the principal protein component of serum, is also contained in tears, which is believed to be derived from serum.[21]

The serum albumin is a multifunctional carrier protein. A number of albumin binding proteins have been identified from endothelium in various tissues.[22,23] One of the albumin binding proteins, gp60, is thought to mediate the transcytosis of albumin,[22] and this protein is shown to be distributed in alveolar epithelium in rat lung.[24] We think that gp60 is also distributed in corneal epithelium to uptake albumin in tears.

The data from rats with intact epithelium under desiccated condition was reported in our previous paper.[15] In that paper, the corneal epithelial disorder superficial punctate keratopathy and erosion were observed in most of the eye under desiccated condition for at least 5 days. However, variations in the frequency of appearance, degree of disorder, and time of appearance were noteworthy in this condition. Thus, to enable us to assess accurately the effect of pharmacological treatments, we attempted to induce uniform corneal epithelial disorder by scraping a small area of the corneal epithelium as a trigger.

Although we did not carry out the measurement of DNA fragmentation and caspase activity in the same cell lines in this study, we already reported in previous studies, in which DNA fragmentation and caspases-3 activity similarly increase in CCL induced by serum deprivation,[17] and in CEPI by etoposide or anti-Fas treatment.

Figure 2 shows 5 mg/ml of albumin is more effective than other concentrations. This result surprised us, because we expected that high concentration of albumin

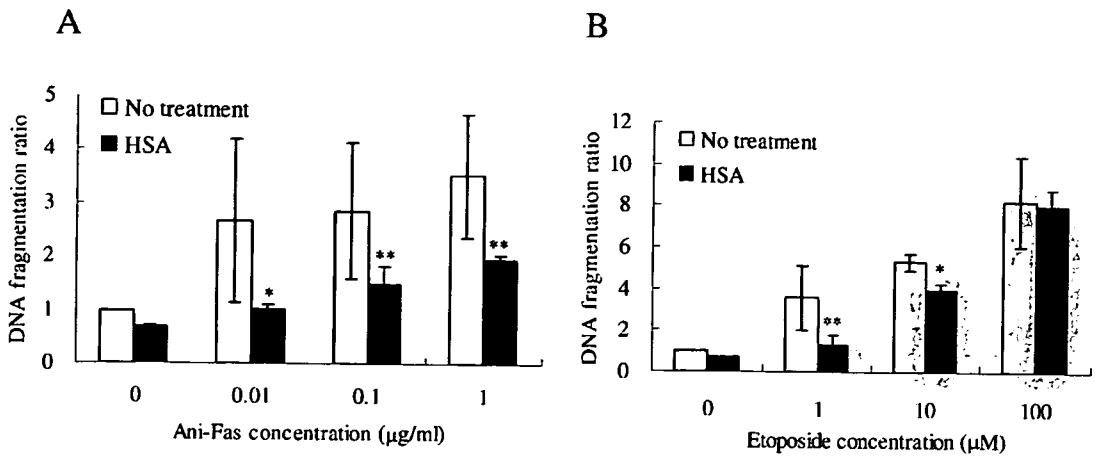

FIGURE 4 Suppression by HSA of apoptosis induced by apoptosis inducer in CEPI. CEPIs were treated with apoptosis inducers in the presence (closed bar) or absence (open bar) of 5 mg/ml HSA. DNA fragmentation, which is an index of apoptosis, was induced by apoptosis inducer, and this fragmentation was suppressed by HSA. (A) Apoptosis was induced by anti-Fas antibody; (B) induced by etoposide. Results are the mean ± SD ($n = 4$). Paired Student's t test was used to determine the significance of differences. *Indicates a significant difference from the result in absence of HSA (no treatment), $p < 0.05$. **Indicates a significant difference for viability from the result in absence of HSA, $p < 0.01$.

was more effective. Growth factors induce growth of cells, otherwise, high concentration of growth factors often suppress cell growth. Furthermore, it was reported that albumin containing fatty acid induced cell death.[25] We think that high concentration of albumin arrests growth of cell or induces cell death. The other reason is the albumin used in this study was purified from human serum. High concentration of HSA and/or contaminated proteins from human serum might act as an antigen in ocular surface of rat, which interferes in recovery of the ocular surface.

It is well-known that withdrawing serum from a medium causes apoptosis in cultured cells, though the precise mechanism is unclear.[26] Anti-Fas antibody induces apoptosis in Fas-expressing cells, and etoposide, which is a topoisomerase II inhibitor, induces apoptosis. These events leading to apoptosis are accompanied by caspase cascade activation.[27] HSA suppressed apoptosis induced by serum deprivation (Fig. 3) or addition of inducers (Fig. 4) in CCL or CEPI. This suppression is not shown in 0.2 mg/ml fibrinogen and 0.02 mg/ml antithrombin (data not shown). In previous studies, bovine serum albumin (BSA) survived from cell death in macrophage or renal tubular cells cultured in survival factors-free medium.[28,29] HSA protected radiation-induced apoptosis accompanied with activation of Akt signaling pathway.[30] Akt has been implicated as a major modulator of cell survival, via the phosphorylation and inactivation of proapoptotic proteins, including the BCL-2 family member BAD12 and Forkhead family transcription factors. The apoptosis suppression effect of albumin may have decreased the area of epithelial defection in the dry eye rats.

Human serum contains many different antioxidants (i.e., ascorbic acid, α-tocopherol, β-carotene, and bilirubin) that may play important roles for general health maintenance. Albumin has also been shown to possess antioxidant activity.[31,32] It was shown that 0.05 and 0.2 mg/ml BSA absorbed the peroxyl radical produced by peroxyl radical generator.[32] This concentration of BSA is comparable with that of HSA suppressing apoptosis in this study (Figs. 3 and 4). Furthermore, BSA was shown to inhibit the accumulation of reactive oxygen species after withdrawal of survival factors.[29] Other functions of albumin were shown, such as esterase-like activity[33] and enolase-like activity.[34] These antioxidant and enzyme activities may be involved with the suppression effect of HSA on apoptosis. Further studies will be required to clear the mechanism of dry eye treatment of HSA.

The precise mechanism of albumin in treatment of dry eye remains unclear. In this study, we present that HSA is useful for clinical treatment of dry eye.

ACKNOWLEDGMENTS

This research was partly supported by a grant-in-aid for research on eye and ear sciences, immunology, allergy and organ transplantation from the Japanese Ministry of Health. We thank Dr. Shigeru Nakamura

(Ophtecs Corporation) for the conduct of the experiment of dry eye model rat.

REFERENCES

[1] Ubels JL, Foley KM, Rismond V. Retinal secretion by the lacrimal grand. *Invest Ophthalmol Vis Sci.* 1986;27:1261–1268.

[2] Ohashi Y, Motokura M, Kinoshita Y, et al. Presence of epidermal growth factor in human tears. *Invest Ophthalmol Vis Sci.* 1989;30:1879–1882.

[3] Van Setten GB, Macauley S, Humphreys-Beher M, et al. Detection of transforming growth factor-alpha mRNA and protein in rat lacrimal glands and characterization of transforming growth factor-alpha in human tears. *Invest Ophthalmol Vis Sci.* 1996;37:166–173.

[4] Yoshino K, Garg R, Monroy D, et al. Production and secretion of transforming growth factor beta (TGF-beta) by the human lacrimal gland. *Curr Eye Res.* 1996;15:615–624.

[5] Wilson SE, Liang Q, Kim WJ. Lacrimal grand HGF, KGF, and EGF mRNA levels increase after corneal epitherial wounding. *Invest Ophthalmol Vis Sci.* 1999;40:2185–2190.

[6] Tsubota K, Goto E, Fujita H, et al. Treatment of dry eye by autologous serum application in Sjogren's syndrome. *Br J Ophthalmol.* 1999;83:390–395.

[7] Higuchi A, Shimmura S, Takeuchi T, et al. Elucidation of apoptosis induced by serum deprivation in cultured conjunctival epithelial cells. *Br J Ophthalmol.* 2006;90:760–764.

[8] Tsubota K, Higuchi A. Serum application for the treatment of ocular surface disorders. *Int Ophthalmol Clin.* 2000;40:113–122.

[9] Matsushita S, Isima Y, Chuang VT, et al. Functional analysis of recombinant human serum albumin domains for pharmaceutical applications. *Pharm Res.* 2004;21;1924–1932.

[10] Kragh-Hansen U, Saito S, Nishi K, et al. Effect of genetic variation on the thermal stability of human serum albumin. *Biochim Biophys Acta.* 2005;1747:81–88.

[11] Fullard RJ. Identification of proteins in small tear volumes with and without size exclusion HPLC fractionation. *Curr Eye Res.* 1988;7:163–179.

[12] Coyle PK, Sibony PA, Johnson C. Electrophoresis combined with immunologic identification of human tear proteins. *Invest Ophthalmol Vis Sci.* 1989;30:1872–1878.

[13] Kuizenga A, van Haeringen NJ, Kijlstra A. SDS-Minigel electrophoresis of human tears. Effect of sample treatment on protein patterns. *Invest Ophthalmol Vis Sci.* 1991;32:381–386.

[14] Shimmura S, Ueno R, Matsumoto Y, et al. Albumin as a tear supplement in the treatment of severe dry eye. *Br J Ophthalmol.* 2003;87:1279–1283.

[15] Nakamura S, Shibuya M, Saito Y, et al. Protective effect of D-beta-hydroxybutyrate on corneal epithelia in dry eye conditions through suppression of apoptosis. *Invest Ophthalmol Vis Sci.* 2003;44:4682–4688.

[16] Stennicke HR, Salvesen GS. Biochemical characteristics of caspases-3, -6, -7, and -8. *J Biol Chem.* 1997;272:25719–25723.

[17] Sharif NA, Wiernas TK, Howe WE, et al. Human corneal epithelial cell functional responses to inflammatory agents and their antagonists. *Invest Ophthalmol Vis Sci.* 1998;39:2562–2571.

[18] Offord EA, Sharif NA, Mace K, et al. Immortalized human corneal epithelial cells for ocular toxicity and inflammation studies. *Invest Ophthalmol Vis Sci.* 1999;40:1091–1101.

[19] Gao J, Gelber-Schwalb TA, Addeo JV, et al. Apoptosis in the lacrimal gland and conjunctiva of dry eye dogs. *Adv Exp Med Biol.* 1998;438:453–460.

[20] Yeh S, Song XJ, Farley W, et al. Apoptosis of ocular surface cells in experimentally induced dry eye. *Invest Ophthalmol Vis Sci.* 2003;44:124–129.

[21] Fukuda M, Wang HF. Dry eye and closed eye tears. *Cornea.* 2000;19:S44–S48.

[22] Schnitzer JE, Oh P. Albondin-mediated capillary permeability to albumin. Differential role of receptors in endothelial transcytosis and endocytosis of native and modified albumins. *J Biol Chem.* 1994;269:6072–6082.

[23] Brunskill NJ. Molecular interactions between albumin and proximal tubular cells. *Exp Nephrol.* 1998;6:491–495.

[24] John TA, Vogel SM, Minshall RD, et al. Evidence for the role of alveolar epithelial gp60 in active transalveolar albumin transport in the rat lung. *J Physiol.* 2001;533(Pt 2):547–559.

[25] Hirashima M, Naruse T, Maeda H, et al. Identification of selenoprotein P fragments as a cell-death inhibitory factor. *Biol Pharm Bull.* 2003;26:794–798.

[26] Evan GI, Brown L, Whyte M, et al. Apoptosis and the cell cycle. *Curr Opin Cell Biol.* 1995;7:825–834.

[27] Enoksson M, Robertson JD, Gogvadze V, et al. Caspase-2 permeabilizes the outer mitochondrial membrane and disrupts the binding of cytochrome c to anionic phospholipids. *J Biol Chem.* 2004;279:49575–49578.

[28] Koh JS, Lieberthal W, Heydrick S, et al. Lysophosphatidic acid is a major serum noncytokine survival factor for murine macrophages which acts via the phosphatidylinositol 3-kinase signaling pathway. *J Clin Invest.* 1998;102:716–727.

[29] Iglesias J, Abernethy VE, Wang Z, et al. Albumin is a major serum survival factor for renal tubular cells and macrophages through scavenging of ROS. *Am J Physiol.* 1999;277:F711–F722.

[30] Jones DT, Ganeshaguru K, Anderson RJ, et al. Albumin activates the AKT signaling pathway and protects B-chronic lymphocytic leukemia cells from chlorambucil- and radiation-induced apoptosis. *Blood.* 2003;10:3174–3180.

[31] DeMaster EG, Quast BJ, Redfern B, et al. Reaction of nitric oxide with the free sulfhydryl group of human serum albumin yields a sulfenic acid and nitrous oxide. *Biochemistry.* 1995;34:11494–11499.

[32] Cao G, Alessio HM, Cutler RG. Oxygen-radical absorbance capacity assay for antioxidants. *Free Radic Biol Med.* 1993;14:303–311.

[33] Kurono Y, Kushida I, Tanaka H, et al. Esterase-like activity of human serum albumin. VIII. Reaction with amino acid p-nitrophenyl esters. *Chem Pharm Bull (Tokyo).* 1992;40:2169–2172.

[34] Drmanovic Z, Voyatzi S, Kouretas D, et al. Albumin possesses intrinsic enolase activity towards dihydrotestosterone which can differentiate benign from malignant breast tumors. *Anticancer Res.* 1999;19:4113–4124.

Microvascular and systemic effects following top load administration of saturated carbon monoxide-saline solution*

Nanae Hangai-Hoger, MD, PhD; Amy G. Tsai, PhD; Pedro Cabrales, PhD; Makoto Suematsu, MD, PhD; Marcos Intaglietta, PhD

Objective: To determine how top loads with different doses of carbon monoxide (CO)-saturated saline solutions (CO-saline) affect microvascular and systemic hemodynamics and to delineate the corresponding biochemical mechanisms.

Design: Prospective study.

Setting: University research laboratory.

Subjects: Male Golden Syrian hamsters.

Interventions: Hamsters implemented with a dorsal window chamber were given different volumes (characterized as percent of blood volume, BV) by intravenous injection of CO-saturated saline.

Measurements and Main Results: Hamsters were observed until 90 mins after infusion of CO-saline solution. In the 20% BV CO-saline infusion group, observation was extended until 180 mins. Systemic variables measured included mean arterial pressure, heart rate, systemic arterial blood gases, and cardiac output and index. Microvascular hemodynamic measurements included vessel diameter, red blood cell velocity, and functional capillary density. Cyclic guanosine monophosphate (cGMP) content in the chamber tissue was measured by enzyme immunoassay. 10% BV of CO-saline increased flow maximally in the microcirculation at 30 mins after infusion (207% in arterioles and 238% in venules, $p < .05$ vs. baseline). Functional capillary density was significantly increased in both 10% and 15% groups ($p < .05$ vs. baseline), and cardiac index increased 130% ($p < .05$ vs. baseline) at 10 mins after 10% CO-saline infusion. There were no changes of microhemodynamic variables and functional capillary density with 2.5%, 5%, and 20% CO-saline infusion during the observation period. Microvascular hemodynamic changes by 10% CO-saline infusion were inhibited completely by L-NAME pretreatment and partially by 1H-[1,2,4]oxadiazole[4,3-a]quinoxqalin-1-one pretreatment. cGMP content in skin fold tissues was related to changes of vessel diameter.

Conclusions: Intravenous injection of CO-saturated saline caused vasodilation and improved microvascular hemodynamics in the hamster window chamber model in a dose-dependent manner. These changes were related to increased cardiac output and local cGMP content. These results support the possible use of CO-saturated solutions as a vasodilator in critical conditions. (Crit Care Med 2007; 35:1123–1132)

Key Words: carbon monoxide; vasodilatation; microcirculation; cyclic guanosine monophosphate; cardiac output; hamster window model

Carbon monoxide (CO) binds to soluble guanylate cyclase (sGC) to increase cyclic guanosine monophosphate (cGMP) in vascular tissue, causing vascular relaxation. Both inhalation and intraperitoneal injection of CO gas cause cardiovascular effects, lowering mean arterial blood pressure (MAP), increasing heart rate (HR), increasing cardiac output, and decreasing total peripheral vascular resistance (1, 2). These effects are present upon the introduction of CO when CO-hemoglobin (CO-Hb) saturation is as low as 7%.

CO is toxic at high dosages and is an effective vasodilator at low dosages that protects cellular species from ischemic damage and inflammation. Its multiple effects suggest that it should be beneficial in the acute treatment of ischemic heart disease, microcirculatory impairment, and ischemic shock. In emergencies requiring blood transfusion, plasma expanders are used until appropriate blood becomes available. In this situation, systemic blood pressure, HR, and respiratory rate are frequently in the normal range while the microcirculation is impaired, a condition not evident from systemic variables. The initial microvascular impairment begins with the decrease of functional capillary density (FCD) (3); the rapid reversal of this process and improvement of microvascular flow are necessary for impeding the progression of irreversible organ damage.

This situation suggests the development of a plasma expander with flow-increasing properties beyond those afforded by the decrease in blood viscosity due to hemodilution. Nitric oxide (NO) is a well-known vasodilator, although it is short lasting. Since endogenous CO functions as a vasodilator, exogenous CO could in principle provide the required vasodilator effect with temporal advantage. Inhalation of CO or intraperitoneal injection of CO gas was beneficial (1, 2); however, these procedures do not lend themselves to accurate dosage. We propose that the intravenous injection of

*See also p. 1213.

From the Department of Bioengineering, University of California, San Diego, La Jolla, CA (NHH, AGT, MI); La Jolla Bioengineering Institute, La Jolla, CA (AGT, PC, MI); and Department of Biochemistry & Integrative Medical Biology, School of Medicine, Keio University, Tokyo, Japan (MS).

Supported, in part, by USPHS Bioengineering Research Partnership grant R24-HL64395, by grants R01-HL62354 and R01-HL62318 (MI), and by Leading Project for Biosimulation from the Ministry of Education, Sciences and Technology of Japan (MS).

The authors have not disclosed any potential conflicts of interest.

For information regarding this article, E-mail: nhangai@bioeng.ucsd.edu

DOI: 10.1097/01.CCM.0000259533.84180.C7

CO-saturated saline (CO-saline) provides a practical and readily quantifiable method for delivering CO to the organism with the aim of increasing microvascular perfusion.

To test our hypothesis, we infused CO-saline solution as top loads to the hamster window chamber model, in different percentages of blood volume, to establish the extent and duration of microvascular and systemic responses and then determine the effectiveness of this methodology in producing dose-dependent vasodilation. In addition, we studied the effects of CO-saline during L-NAME and the sGC inhibitor 1H-[1,2,4]oxadiazole[4,3-a]quinoxqalin-1-one (ODQ) treatment to delineate the corresponding biochemical pathways.

MATERIALS AND METHODS

Animal Preparation

Investigations were performed in male Golden Syrian hamsters (Charles River Laboratories, Boston, MA) according to the procedures outlined in the *Guide for the Care and Use of Laboratory Animals* (National Research Council, 1996) and were approved by the local animal subjects committee. The hamster window chamber model is widely used for microvascular studies in the unanesthetized state, and the complete surgical technique is described elsewhere (4). Catheters (PE-50) were implanted in the carotid artery and jugular vein. Experiments were performed after at least 24 hrs but within 48 hrs after catheter implantation. Both procedures were performed under anesthesia (Nembutal, 50 mg/kg, intraperitoneal injection, Abbott, Abbott Park, IL).

Systemic Variables

MAP was tracked continuously during the experimental period, and HR was determined from the pressure trace (Biopac, Santa Barbara, CA; Spectramed Pressure Transducer). Hematocrit was measured from centrifuged arterial blood samples taken in heparinized capillary tubes.

Blood Chemistry

Arterial blood was sampled from the carotid artery catheter into heparinized capillary tubes and immediately analyzed for Po_2, Pco_2, and pH at 37 EC (pH/Blood Gas Analyzer, 248, Bayer). Hemoglobin concentration was measured using a photometer (B-Hemoglobin, Hemocue, Sweden).

Microhemodynamic Variables

The unanesthetized animal was placed in a restraining tube attached to the stage of an inverted microscope (IMT-2 Olympus, New Hyde Park, NY) equipped with ×20 objective (Leitz PHARCO L1, n.a. 0.32). The tissue image was projected onto a CCD camera (COHU 4815-2000, COHU, San Diego, CA), video recorded (Panasonic AG-7355,) and viewed on a Sony monitor (PVM-1271Q).

Microhemodynamics. Arteriolar and venular blood flow velocities were measured using the photodiode cross-correlation method (5) (Photo Diode/Velocity Tracker 102B, Vista Electronics, San Diego, CA). The measured centerline velocity (V) was corrected according to vessel size to obtain mean red blood cell (RBC) velocity (6). A video image-shearing method was used to measure vessel diameter (D) (7). Blood flow (Q) was calculated from the measured values as $Q = V\ H\ B(D/2)^2$.

Arterioles and Venules. Microvessels were classified according to their position in the microvascular network (3) including large feeding arterioles, small arcading arterioles, large venules, and small collecting venules (8).

Functional Capillary Density. Capillaries are considered functional if RBCs transit through the capillary segments during a 45-sec period. FCD was tabulated from the capillary lengths with RBC transit in an area comprising ten successive microscopic fields (420 × 320 μm^2).

Saturated CO-Saline Solution

Normal saline (0.9% NaCl) was bubbled with 100% CO (Airgas, Radnor, PA) for 20 mins at room temperature and atmospheric pressure resulting in a concentration of about 0.93×10^{-4} M (CO = 28.01 molecular weight and 0.0026 g/100 mL solubility in water at 20°C) and a maximal possible HbCO concentration of 1% for a 10% top load.

Circulatory Carboxy Hemoglobin Concentration

CO-Hb concentration in systemic venous blood was measured spectrophotometrically according to Parks and Worth (9). The second derivative spectrum was determined between 390 and 450 nm using a UV/VIS Spectrometer (Lambda 20, Perkin Elmer, Wellesley, MA), and data were analyzed using the standard curve from normal hamster samples.

cGMP Content in the Skin Fold

Concentration of cGMP in the skin tissue was determined using a commercial enzyme immunoassay kit (Enzymeimmunoassay Biotrak System, Amersham Biosciences, Piscataway, NJ). Tissues were snap-frozen in liquid nitrogen immediately after dissection from the anesthetized animals. Samples were stored at −80°C until analysis. Assays were per-

Table 1. Mean arterial pressure (MAP) and heart rate (HR) as a function of the amount of carbon monoxide (CO)-saline delivered by top load

	No.	BL	10 Mins	30 Mins	60 Mins	90 Mins
MAP, mm Hg						
10% TP	4	112 ± 10	112 ± 14	116 ± 16	110 ± 7	114 ± 11
20% TP	4	121 ± 8	122 ± 12	117 ± 5	117 ± 6	114 ± 5
2.5% CO	5	110 ± 8	111 ± 8	109 ± 6	107 ± 8	106 ± 9
5% CO	4	120 ± 15	121 ± 13	119 ± 11	119 ± 14	118 ± 14
10% CO	5	115 ± 9	113 ± 9	112 ± 10	109 ± 9	107 ± 6[a]
15% CO	5	112 ± 11	107 ± 12	103 ± 9[a]	100 ± 7[a]	103 ± 7[a]
20% CO	4	112 ± 3	110 ± 1	107 ± 5	107 ± 6	108 ± 6
HR, beats/min						
10% TP	4	404 ± 8	387 ± 10	397 ± 28	408 ± 22	413 ± 33
20% TP	4	412 ± 50	381 ± 42	388 ± 37	383 ± 33	389 ± 33
2.5% CO	5	412 ± 22	423 ± 27	426 ± 9	413 ± 18	412 ± 30
5% CO	4	388 ± 21	386 ± 50	405 ± 58	434 ± 27	400 ± 37
10% CO	5	443 ± 27	421 ± 32	427 ± 34	429 ± 29	414 ± 45
15% CO	5	429 ± 52	396 ± 60	406 ± 44	359 ± 51	364 ± 15
20% CO	4	431 ± 54	420 ± 53	420 ± 52	415 ± 53	404 ± 36

BL, baseline; 10% TP, top load of 10% blood volume of saline (= 0% CO); 20% TP, top load 20% blood volume of saline.
[a]$p < .05$ vs. baseline.